Computational Materials Science 160 (2019) 256–274

Contents lists available at ScienceDirect

Computational Materials Science

journal homepage: www.elsevier.com/locate/commatsci

The variable node multiscale approach: Coupling the atomistic and continuum scales

Omid Alizadeh, Soheil Mohammadi*

High Performance Computing Laboratory, School of Civil Engineering, Faculty of Engineering, University of Tehran, Tehran, Iran

ARTICLE INFO

Keywords:
Multiscale
Variable node
Displacement decomposition

ABSTRACT

Linking atomistic and continuum zones in multiscale methods is a necessity in order to overcome the deficiencies of the conventional molecular and continuum-based methods. In this paper, a novel approach is presented to bind the atomistic and continuum zones together based on the combined concepts of the finite element method and the radial point interpolation meshfree method. This variable node multiscale method (VNMM) introduces a new way to couple the finite element method with the molecular solutions with nodes coinciding with the atoms. In contrast to QC methods, VNMM does not need a mesh refinement in the vicinity of the molecular zone, nor it requires an overlapping zone in the continuum/atomistic interface which is necessary in bridging schemes. In VNMM, the total displacement of each atom is decomposed into coarse and fine displacements, in which the coarse displacement is computed using the finite element solution over the whole domain, while the fine displacement is calculated just in a limited atomistic zone with the use of molecular statics. Integration of the finite element method within the VNMM formulation potentially allows for enrichment of any field over the entire domain. Conventional interatomic potentials could be employed at the atomistic zone. The results are compared with the fully atomistic simulation, conducted with the molecular statics, and the multiscale quasicontinuum method. A good agreement is observed with substantially reduced degrees of freedom and computational costs.

1. Introduction

Scientists have always been interested in exploring how macroscopic or engineering continuum-based phenomena are formed from atomistic responses [1]. Nevertheless, high computational costs of fully atomistic simulations [2] compelled them to utilize the multiscale methods in which efficiency of two or more scales are combined to obtain a level of near atomic-scale accuracy with affordable computational costs.

Concurrent multiscale methods, developed in the past two decades [3], can be categorized into two different types based on to the adopted method for coupling of atomic and continuum zones [4]. The first type, called “strong coupling”, includes methods with nodes coinciding atoms in the desired domain, while in “weak coupling”, as the second type, no coincidence is needed. Clearly, the coincidence of nodes and atoms makes a strong constraint between them but requires refinement of the mesh to the atomic lattice size near the interface of two scales.

One of the earliest concurrent multiscale methods with a strong coupling is the quasicontinuum (QC) method, developed by Tadmor et al. [5] based on the Cauchy-Born rule (CBR). This method has been frequently used by researchers in a wide range of subjects such as crack propagation [6–9], nanoindentation [10,11], modeling of irregular lattices [12], nanocontact [13], surface effects [14], etc. QC divides the entire domain into local and nonlocal zones. Atoms exist in both zones but with different characteristics. Some atoms, called the representative atoms, have degrees of freedom to compute the total energy of the domain, while the others do not have any degrees of freedom and their energy is taken into account by the energy of representative atoms. As a result, QC reduces the number of degrees of freedom from the huge number of atoms to just a limited number of representative atoms. Despite being very efficient, a complex algorithm of mesh refinement in the nonlocal zone should be implemented.

Many researchers have modified the original QC method in order to perform finite temperature simulations [15,16], higher order Cauchy-Born implementation [17,18], summation rule modification [19,20], ghost force correction [21,22], and modeling of multi-lattice materials [23,24].

To avoid complicated and expensive mesh refinements, many concurrent multiscale methods have been developed; among them, the bridging domain method (BDM) developed by Xiao and Belytschko [25] and the bridging scale method (BSM) developed by Wagner and Liu [26] are better known. Both methods do not require the coincidence of

* Corresponding author.
E-mail address: smoham@ut.ac.ir (S. Mohammadi).

https://doi.org/10.1016/j.commatsci.2019.01.003
Received 6 October 2018; Received in revised form 25 December 2018; Accepted 4 January 2019

atoms and nodes. In other words, the positions of nodes are independent of positions of atoms and no mesh refinement is needed.

In BDM, the whole domain is decomposed into a continuum and molecular dynamics zones, with an overlapped band, called the handshake region. The compatibility condition between these two domains is established by the displacement constraints using the Lagrange multiplier approach [27]. Many researches have tried to couple the extended finite element method and the molecular dynamics approach with the use of BDM [28]. Although the weak coupling of BDM via the Lagrange multiplier eliminates the difficulties of mesh refinement, spurious forces, especially in dynamic systems, are generated, which result in some errors in the final response and reduction of accuracy.

In BSM, the finite element mesh is present everywhere in the whole domain and the molecular dynamics (MD) is placed locally in the desired area. The total displacement of an atom is decomposed into the coarse and fine-scale displacements. The fine-scale displacement is the difference between the molecular dynamics displacement and that of the finite element method. Atoms and nodes do not require to coincide in this method [29].

Both BDM and BSM methods eliminate some of the shortcomings of the methods with strong coupling. Investigations, however, have shown that the error of bridging methods, for example, in a specific fracture modeling of nickel, is more than that of QC [30].

Strong and weak coupling methods use molecular statics or molecular dynamics in the atomistic zone to calculate the energy and displacement filed of the proposed zone. For calculating the energy of the continuum zone, the finite element method is used in BDM and BSM, while the energy in QC is computed by summation of the energy of all atoms.

Due to the fact that meshfree methods could well perform in discontinuous regions, especially for large atomic simulations, many efforts have been made to couple meshfree methods with molecular statics/dynamics with strong or weak coupling schemes. In a recent attempt, Kochmann et al. developed a meshfree quasicontinuum method [31] by using the concepts of meshfree methods in the local zone. The method eliminated the need for any elements in the domain, but it suffered from the generation of nonphysical spurious forces. Moreover, the Cauchy-Born hypothesis could not be directly applied, as it was used in QC methods.

Moreover, Wang et al. introduced a method to couple the meshless element-free Galerkin (EFG) method with molecular dynamics [32]. In this method, however, the efficiency of the meshless method was not used to completely eliminate the spurious forces in the handshake region, and EFG was used just as a more accurate alternative to the conventional finite element method. Moreover, the moving least square (MLS) shape functions of EFG caused some difficulties in enforcing the essential boundary conditions.

Except the well-known BD, BS and QC concurrent methods, some novel approaches have been established to couple the two atomistic and continuum zones [33]. An adaptive multiscale method (AMM), developed by Budarapu et al. [34], introduces a weak coupling scheme along with an adaptive algorithm in the continuum zone to coarsen the refine zone. The atomistic area is solved by the molecular statics and a fixed boundary is applied by the use of ghost atoms.

In this paper, a new method, called the variable node multiscale method (VNMM), is presented based on the meshfree concepts and the strong coupling form of coincidence of atoms and nodes, while no complex mesh refinement algorithm is required and the need for the existence of an overlapping domain is avoided. In VNMM, the molecular statics is used in the localized atomistic zone to calculate and minimize the energy, while the energy of the far filed is essentially based on the conventional finite elements formulations (similar to any finite element modeling of macro problems) or the atomistic potential energy of the underneath atoms (similar to QC method in far regions [5]). First, the proposed method is explained with a discussion on implementation issues. Various examples are then simulated to assess the accuracy and performance of the developed VNMM.

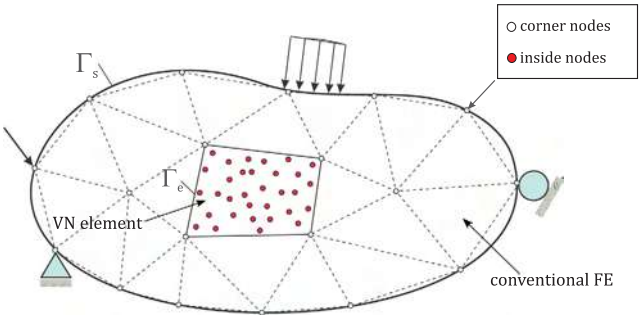

Fig. 1. A typical variable node element.

2. Variable node multiscale method

2.1. Fundamentals

Coupling the continuum and atomistic zones can be established by a limited number of methods in the forms of either strong or weak coupling. A strong coupling ensures the high accuracy of response, but with the expense of mesh refinement and redundant degrees of freedom.

To avoid remeshing, the size of all elements can be kept unchanged while some additional nodes are added inside an element (See Fig. 1). If the additional nodes are positioned in the atomic position, they can function simultaneously as both nodes and atoms. For this purpose, a combination of concepts of the conventional finite element and meshfree methods can be used, as recently reported in the form of the variable node element (VNE) [35]. The variable node element consists of 4 nodes on the corners and some internal nodes, known as the inside nodes. In a variable node element, the number of inside nodes could vary from one element to another, and with the completely different nodal arrangement. The variable node element has successfully been used in the finite element simulation of various continuum (single scale) problems [35]. The complete procedure of derivation of shape functions is explained in Section 2.3.

If the variable node element is tuned with the following conditions, it could be used as a multiscale element:

I. The element should perform similar to conventional elements along its edges to ensure continuity and compatibility conditions at the boundaries.
II. Inside nodes should not be placed on the boundaries of VN element.
III. The arrangement of inside nodes must be similar to the arrangement of atomic lattices. Any defect like inclusion, crack, hole and grains can be modeled using corresponding arrangements of inside nodes.

Accordingly, the new multiscale element is called the “variable node multiscale element (VNME)”. Fig. 2 shows a number of typical arrangements of atoms for the positions of inside nodes. Fig. 2a, which shows a randomly distributed arrangement of nodes, can be used for finite element simulation of higher order fields, whereas distributions of the inside nodes in Fig. 2b and c allows for the element to be used as a variable node multiscale element to simulate FCC and Graphene structures, respectively.

In VNMM, an arbitrary mesh is generated on a molecular setup, as typically shown in Fig. 3. In the vicinity of the zone in which the atomic accuracy is required, a number of variable node multiscale elements are placed and all the atoms within these elements are given full degrees of freedom. In VNMM, atoms could be modeled everywhere, but modeling of atoms which are located in the cutoff zone of inside nodes of variable node multiscale elements is necessary. In other words, unlike QC, there is no need to model all atoms in VNMM. If atoms are considered in the

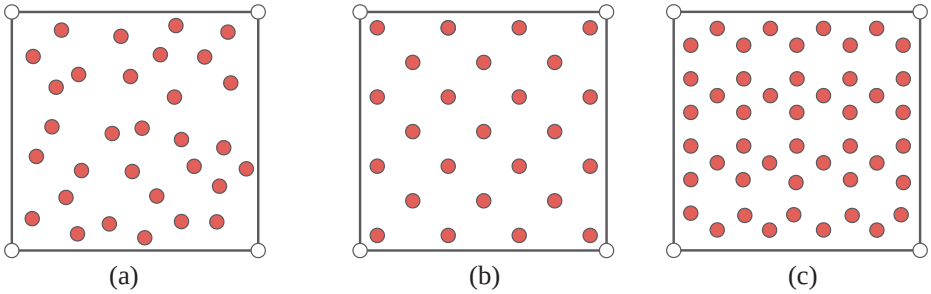

Fig. 2. Variable node multiscale element; (a) randomly distributed inside nodes, (b) FCC structure of inside nodes, (c) Graphene structure of inside nodes.

whole VNMM model, the constrained atoms far from the inside nodes of variable node multiscale elements (gray atoms in Fig. 3b which are not in the cutoff zone of inside nodes of VNME) do not affect the accuracy, while in Fig. 3c the gray atoms, considered only in neighboring elements of the VN multiscale element, are inside the cutoff zone of inside nodes and have a major contribution and directly affect the procedure of computing the final position of inside nodes/atoms.

Those atoms that are inside nodes of the variable node multiscale element (red circles in Fig. 3) are free to move and have degrees of freedom in all directions. In contrast, the atoms beneath the conventional finite elements do not have any independent degrees of freedom and move according to the deformation gradient of their parent elements. The Cauchy-Born rule [36] demonstrates that the new position of these atoms for crystalline materials ($\boldsymbol{x}_i^{atom}$) is derived from Eq. (1),

$$\boldsymbol{x}_i^{atom} = \boldsymbol{F}\boldsymbol{X}_i^{atom} \tag{1}$$

where $\boldsymbol{F}$ is the deformation gradient of the element and $\boldsymbol{x}_i^{atom}$ and $\boldsymbol{X}_i^{atom}$ are the final and initial positions of the ith atom, respectively.

In the variable node multiscale method, a linear or nonlinear form

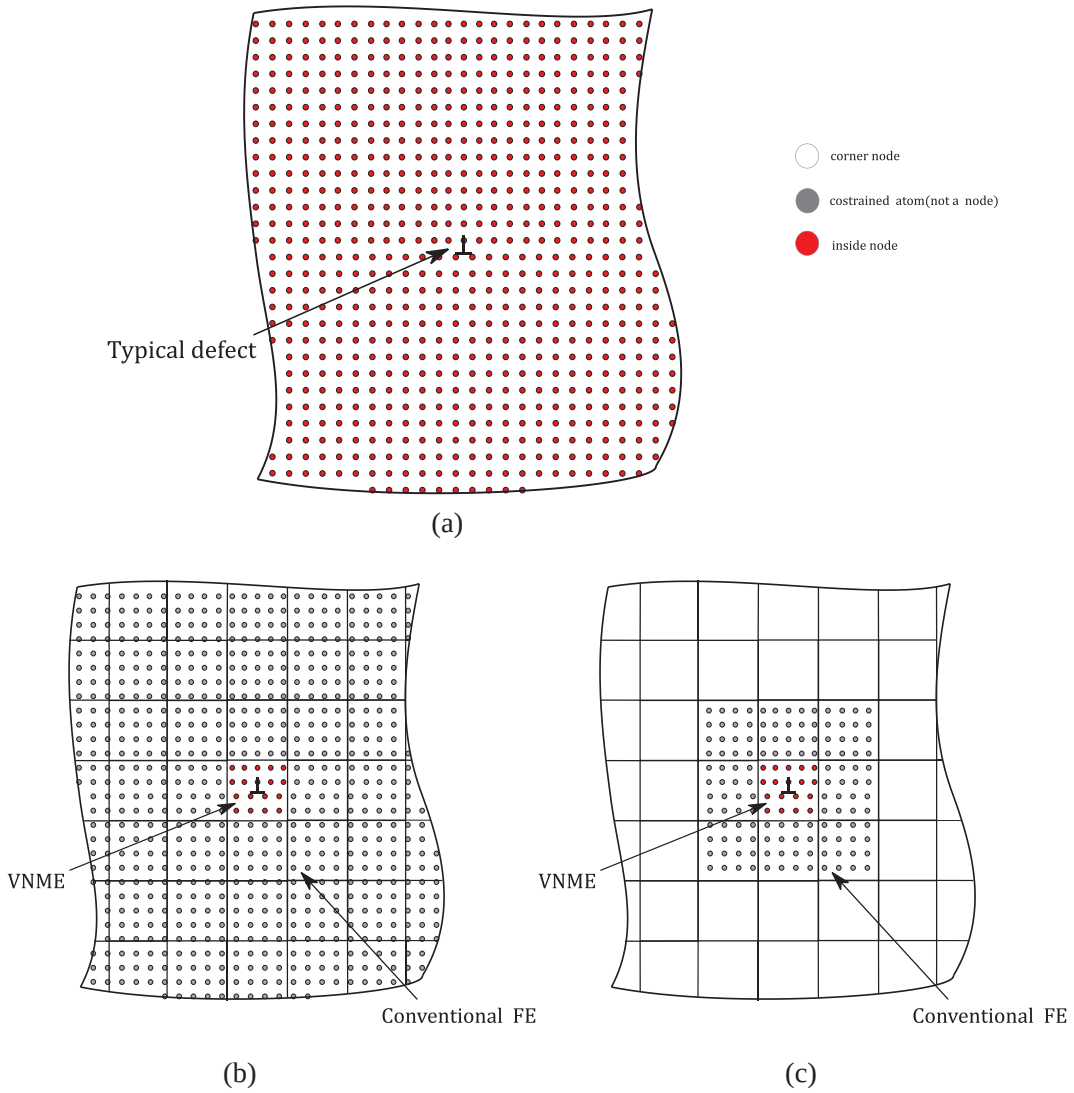

Fig. 3. (a) Schematic molecular setup with a typical defect, (b) VNMM with modeling of all atoms (similar to QC), (c) VNMM with partial modeling of atoms (similar to BDM and BSM concepts).

of the finite element method could be used. First, the zones with some kind of defects or high gradient in the desired field are simulated using the variable node multiscale element, while the rest of the domain is modeled by the conventional finite elements (See Fig. 3b). The energy of the whole domain, including VN elements and conventional finite elements, should be minimized. Displacement of all nodes is accordingly calculated by solving the governing virtual work (weak form) of the finite element model.

2.2. Formulation and implementation

Consider a domain with full atoms, as typically shown in Fig. 3b. The total energy of the model (Π) is,

$$\Pi(\boldsymbol{u}) = \sum_{i=1}^{N_e^{conv}} W(\boldsymbol{F}_i(\boldsymbol{u}))\Omega_i + \sum_{j=1}^{N_e^{VNME}} W(\boldsymbol{F}_j(\boldsymbol{u}))\Omega_j - \sum_{k=1}^{N_n} \boldsymbol{f}_k^{ext}\cdot\boldsymbol{u}_k \tag{2}$$

where W is the strain energy density function, $\boldsymbol{F}$ is the deformation gradient, Ω is the volume of the element, $\boldsymbol{f}^{ext}$ is the external force vector applied on a node, N_n is the total number of nodes, N_e^{conv} and N_e^{VNME} are the number of conventional finite elements and variable node multiscale elements, respectively.

In VNMM, the conventional FE should be used in regions with rather uniform deformation. Therefore, despite the dependency of the strain energy function ($W(\boldsymbol{F})$) to the adopted continuum-based constitutive law (employed in the FE procedure) according to the Cauchy-Born rule [36], the first term of the right-hand side of Eq. (2) can be assumed equal to the energy of all underneath atoms (constrained atoms under conventional finite elements).

$$\sum_{i=1}^{N_e^{conv}} W(\boldsymbol{F}_i(\boldsymbol{u}))\Omega_i \approx \sum_{\alpha=1}^{N_a^{conv}} U_\alpha \tag{3}$$

U_α is the energy of an atom and N_a^{conv} is the number of atoms under conventional finite elements (gray atoms in Fig. 3).

It should be noted that the procedure of Eq. (3) is not similarly valid for the variable node multiscale elements due to the fact that the deformation gradient over the VNME is not uniform and the Cauchy-Born rule cannot be employed [37]. This is numerically examined with an example in Section 2.4.

It should be noted that the energy of atoms under the variable node multiscale elements, which is computed with the summation of interatomic potentials, is not identical to that of the VNME calculated from the finite element method based on continuum constitutive laws due to the non-uniformity of the deformation gradient of VNME. Accordingly, an energy correction term ($\widetilde{\Pi}$) is needed:

$$\sum_{\alpha=1}^{N_a^{VNME}} U_\alpha \approx \sum_{j=1}^{N_e^{VNME}} W(\boldsymbol{F}_j(\boldsymbol{u}))\Omega_j + \widetilde{\Pi} \tag{4}$$

The purpose of VNMM is to achieve higher accuracy based on the interatomic energy computation. Solution of Eq. (2), which does not include the energy correction term ($\widetilde{\Pi}$), is accurate only for all nodes of the conventional finite element. For inside nodes of VNME, however, correction of energy and displacement is necessary. Since the major part of the energy could be calculated by Eq. (2), its corresponding solution is called as coarse displacement ($\boldsymbol{u}^{coarse}$). The deformed position of underneath atoms in conventional finite elements is calculated using the Cauchy-Born rule [38].

Fig. 4a shows a typical setup of VNMM with one VNME in the middle and 8 conventional FE elements. Displacements of all nodes after the FEM analysis, as shown in Fig. 4b, represent the coarse approximation of displacement ($\boldsymbol{u}^{coarse}$). According to Fig. 4b, atoms under the conventional finite elements are positioned in their correct position by applying Eq. (1), but inside nodes/atoms of variable node multiscale element may not be placed at their accurate position, unless the energy correction part ($\widetilde{\Pi}$) is considered.

The difference in the final displacement with the solution of Eq. (2) for the inside nodes/atoms of VNME arises from the fact that the strain energy density function of VNME is based on the continuum based constitutive equations, which is not necessarily consistent with the interatomic potential function of atoms. In order to find the correct position of inside nodes/atoms after applying the coarse displacement and to eliminate the error of displacement of VNME inside nodes/atoms, the fine-tuned displacements of inside nodes/atoms (called the fine displacement, $\boldsymbol{u}^{fine}$) is calculated. This is achieved by minimizing the energy of the inside nodes/atoms based on the atomic solutions:

$$\widetilde{\Pi}(\boldsymbol{u}^{fine}) = \sum_{\alpha=1}^{N_a^{VNME}} U_\alpha(\boldsymbol{X}_\alpha + \boldsymbol{u}^{coarse} + \boldsymbol{u}^{fine}) \tag{5}$$

where $\widetilde{\Pi}(u^{fine})$ is the total energy of the inside nodes/atoms, U_α is the energy of the ith inside node/atom derived from the interatomic potential and N_a^{VNME} is the total number of inside nodes/atoms in all variable node multiscale elements.

It should be noted that the coarse displacement of atoms in Eq. (5) is completely calculated by minimization of Eq. (2) and it is, therefore, can be considered as a known term. To further clarify the point, Eq. (2) is rewritten in terms of the coarse and fine displacements,

$$\Pi(\boldsymbol{u}) = \sum_{j}^{N_{VNME}} W(\boldsymbol{F}(\boldsymbol{u}^{coarse}))\Omega_j + \widetilde{\Pi}(\boldsymbol{X}_\alpha + \boldsymbol{u}^{coarse}, \boldsymbol{u}^{fine}) + \sum_{j}^{N_{conv}} W(\boldsymbol{F}(\boldsymbol{u}^{coarse}))\Omega_j - \sum_{k}^{N_n} f_k^{ext}\cdot u_k \tag{6}$$

To compute the coarse and fine displacements, Eq. (6) should be minimized with respect to $\boldsymbol{u}^{coarse}$ and $\boldsymbol{u}^{fine}$,

$$\frac{\partial\Pi(u)}{\partial\boldsymbol{u}^{coarse}} = \frac{\partial\left(\sum_j^{N_{VNME}} W(\boldsymbol{F}(\boldsymbol{u}^{coarse}))\Omega_j\right)}{\partial\boldsymbol{u}^{coarse}} + \frac{\partial(\widetilde{\Pi}(\boldsymbol{X}_\alpha + \boldsymbol{u}^{coarse}, \boldsymbol{u}^{fine}))}{\partial\boldsymbol{u}^{coarse}} + \frac{\partial\left(\sum_j^{N_{conv}} W(\boldsymbol{F}(\boldsymbol{u}^{coarse}))\Omega_j\right)}{\partial\boldsymbol{u}^{coarse}} + \frac{\partial(\sum_k^{N_n} f_k^{ext}.\ u_k)}{\partial\boldsymbol{u}^{coarse}} = 0 \tag{7}$$

$$\frac{\partial\Pi(u)}{\partial\boldsymbol{u}^{fine}} = \frac{\partial(\widetilde{\Pi}(\boldsymbol{X}_\alpha + \boldsymbol{u}^{coarse}, \boldsymbol{u}^{fine}))}{\partial\boldsymbol{u}^{fine}} = 0 \tag{8}$$

Eqs. (6) and (7), which include derivatives of the common term ($\widetilde{\Pi}(\boldsymbol{X}_\alpha + \boldsymbol{u}^{coarse}, \boldsymbol{u}^{fine})$) with respect to both the coarse and fine displacements, should be solved simultaneously.

Since the internal energy is a path-independent state function [39], the total energy of the system based on the interatomic potential, can be minimized in a two-step approach based on Eqs. (7) and (8), as typically shown in Fig. 4. In Eq. (7), the initial position is known and the coarse displacement is computed, while in Eq. (8), the initial position and coarse displacement of atoms are known and the fine displacement is determined.

Therefore, in the variable node multiscale method, displacement of an inside node/atom can be decomposed into the finite element (coarse) and molecular statics (fine) solutions:

$$\boldsymbol{u}^{total} = \boldsymbol{u}^{coarse} + \boldsymbol{u}^{fine} \tag{9}$$

Fig. 4c demonstrates the final position of all nodes and atoms. In this figure, inside nodes/atoms of the variable node multiscale element are moved to their correct position, while the atoms beneath the conventional finite elements remain unchanged after applying the coarse displacement. In other words, the fine displacement of atoms under conventional finite elements is equal to zero due to the Cauchy-Born rule.

To further discuss the implementation of the method, first, a complete list of neighboring atoms is created for each inside node/atom of the VNME. The list includes both grey and red atoms in the cutoff, as shown in Fig. 5. It is essential to account only for the atoms beneath the conventional finite elements which are in the cutoff range of VNME inside nodes/atoms. Considering other atoms in Eq. (5) does not affect

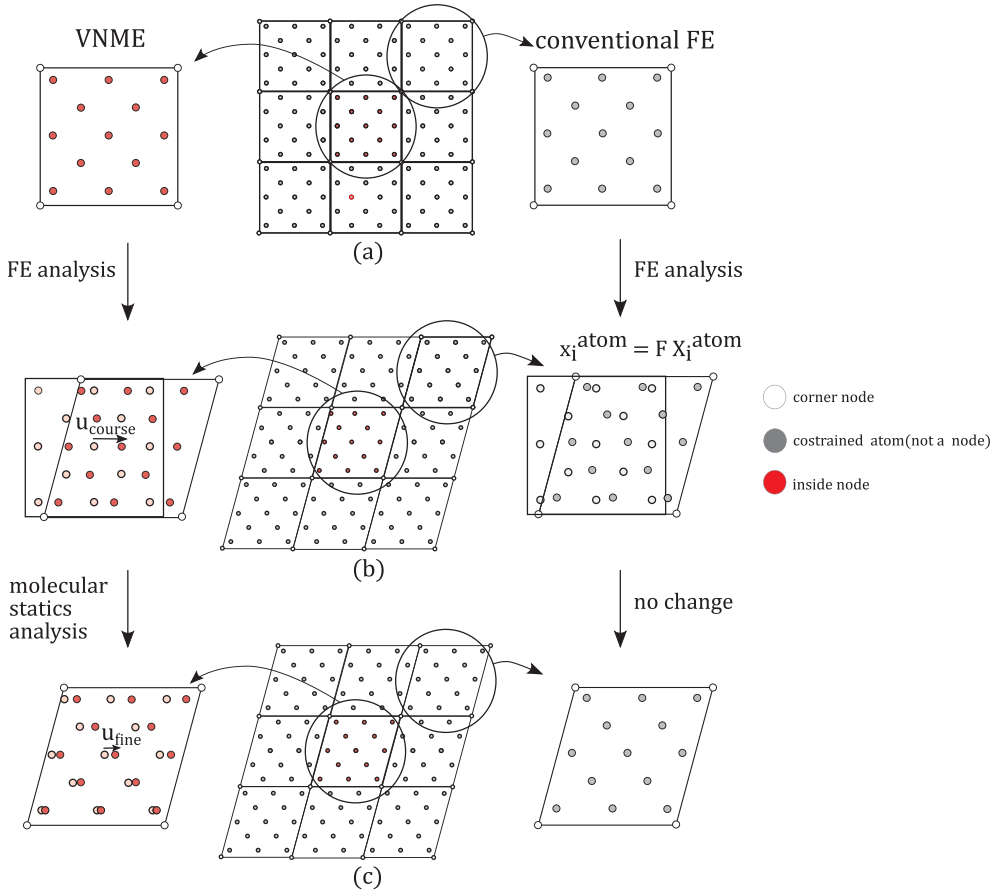

Fig. 4. (a) Initial VNME setup, (b) after FEM analysis of the domain, (c) after minimizing the energy of inside nodes by molecular statics.

the accuracy of the response but increases the computational time. Moreover, as depicted in Fig. 5, the inside node/atom of the variable node multiscale element, which is labeled as "1", should have neighboring nodes/atoms within the cutoff radius, whose exact positions are yet to be calculated. In contrast, the exact positions of some atoms in the neighboring of the node/atom labeled as "2" are well defined from the CB rule of adjacent conventional FE elements. In other words, the gray atoms in the neighboring of the "2" atom are assumed to be located in their correct final positions, but the red ones in the vicinity of the "2" atom are not in their exact positions. This is due to the fact that the position of gray atoms within the atom "2" cutoff is calculated using the Cauchy-Born rule, which is assumed sufficiently accurate. Therefore, the number of atoms which should be considered in the energy minimization Eq. (5) is limited to the number of inside nodes of the variable node multiscale element. It should be mentioned that the number of inside nodes which are located in the cutoff zone of another inside node, is not constant and varies according to the cutoff radius and the location of the inside node of the variable node multiscale element. These important aspects will later be discussed in numerical simulations.

In VNMM there is no limitation either in the number of inside nodes or in the number of variable node elements. In the extreme case of using variable node elements with full inside nodes in the entire domain, the number of inside nodes (N_{inside}) becomes equal to the atoms/molecules of a molecular statics simulations. Since the reduction of computational costs in multiscale methods is a significant issue, the prementioned extreme model is not recommended for such problems.

After minimizing Eq. (8), the positions of inside nodes are changed, and the shape functions and stiffness matrix of VNME should be updated and re-assembled in the global stiffness matrix. This is due to the

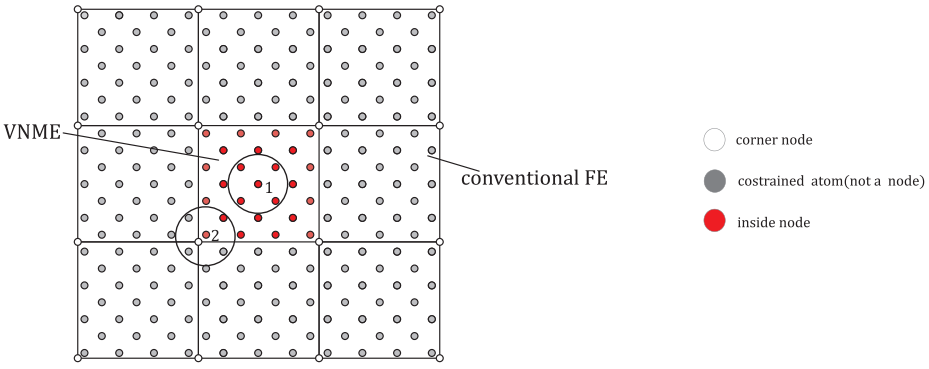

Fig. 5. A typical setup of a multiscale problem with FCC structure.

Box 1
Algorithm of VNMM.

1. *Initialize the mesh and locate the variable node multiscale elements*
1.1. *set the initial node positions* $\boldsymbol{x}_0$
2. **Loop** $i = 1$ to $\boldsymbol{N_{time}}$ *(total number of time steps)*
2.1. **Loop** $j = 1$ to $\boldsymbol{N_{FE}}$ *(number of All conventional FE)*
2.2. *Establish the shape functions of FE elements*
2.3. *Generate the stiffness matrix and assemble in global stiffness matrix*
2.4. *Apply the loading and boundary conditions*
2.5. **end**
2.6. **Loop while** *not converged*
2.7. **Loop** $j = 1$ to $\boldsymbol{N_{VNME}}$ *(number of All VNME)*
2.8. *Establish the shape functions of VN multiscale elements*
2.9. *Generate the stiffness matrix and Update in global stiffness matrix*
2.10. **end**
2.11. *Compute the coarse displacement of FEM nodes* $(\boldsymbol{u^{coarse}})$ *from Eq. (7)*
2.12. $\boldsymbol{x_i^{node} = X_i^{node} + u^{coarse}}$
2.13. **Loop** $k = 1$ to $\boldsymbol{N_{FE}}$ *(number of conventional finite elements with underneath atoms)*
2.14. *Compute the deformation gradient of the element* $(\boldsymbol{F_k(x_i^{node})})$
2.15. **Loop** $m = 1$ to $\boldsymbol{N_{atom}^k}$ *(number of atoms under the kth element)*
2.16. $\boldsymbol{x_m^{atom} = F_k X_m^{atom}}$
2.17. **end**
2.18. **end**
2.19. *Compute* $\widetilde{\Pi}(\boldsymbol{u^{fine}}) = \sum_{\alpha=1}^{N_\alpha^{VNME}} \mathbf{U}_\alpha(\boldsymbol{X_\alpha + u^{coarse} + u^{fine}})$
2.20. *Compute the fine displacement* $(\boldsymbol{u^{fine}})$ *for inside atoms by minimizing* $\widetilde{\Pi}(\boldsymbol{u^{fine}})$
2.21. $\boldsymbol{u_{insideatom}^{total} = u_{insideatom}^{coarse} + u_{insideatom}^{fine}}$
2.22. **Loop** $n = 1$ to $\boldsymbol{N_{inside}}$ *(total number of inside nodes/atoms)*
2.23. $\boldsymbol{x_n^{insideatom} = X_n^{insideatom} + u_n^{total}}$
2.24. **end**
2.25. *Check the convergence criterion*
2.26. **end loop while**
2.27. *Compute the stress filed from* $\boldsymbol{u^{total}}$ *by conventional procedures*
3. **end**

fact that the shape functions of the variable node multiscale element are related to the position of inside nodes.

Box 1 briefly explains the implementation procedure of the proposed variable node multiscale method.

2.3. Variable node element

In order to establish the variable node element, the shape functions of all inside nodes should be created. For this purpose, a combination of meshfree concept and the conventional finite element method is used. In other words, the positions of nodes on the boundary of the element are similar to the conventional elements, and the inside nodes are dealt with as nodes of the meshfree method. So, a combination of mesh free method and the finite element is used to create the shape functions of all nodes. Since the polynomial basis functions are very sensitive to the position of nodes and have potential singularities in calculating the moment matrix [40], the radial basis functions are adopted to form the shape functions.

Approximation by the radial point interpolation method (RPIM) can be written as,

$$\psi_i(\boldsymbol{x}) = \sum_{j=1,j\neq i}^{N_b+N_{inside}} R_j(\boldsymbol{x})\lambda_j(\boldsymbol{x}_i) = \boldsymbol{R}^T(\boldsymbol{x})\boldsymbol{\lambda}(\boldsymbol{x}_i) \tag{10}$$

where $\psi_i(\boldsymbol{x})$ is the shape function of the ith node, R is the radial basis function, which could be selected from Table 1, and λ is the unknown coefficient. N_b and N_{inside} are the number of nodes on the boundary and inside of the element, respectively.

Since the shape functions derived from Eq. (10) are not continuous across the interface of two adjacent elements, a modification is applied to ensure C^0 continuity. For this aim, a ramp function $\varphi(\boldsymbol{x})$ is used to make a smooth combination of ψ_i and conventional shape functions $N_i(\boldsymbol{x})$,

Table 1
Radial basis functions.

RBF	Mathematical Form
Multi-Quadrics (MQ) [41]	$R_i(x, y) = (r_i^2 + C^2)^q = [(x - x_i)^2 + (y - y_i)^2 + C^2]^q$
Gaussian (EXP) [42]	$R_i(x, y) = \exp(-cr_i^2) = \exp\{-c[(x - x_i)^2 + (y - y_i)^2]\}$
Thin plate spline (TPS) [43]	$R_i(x, y) = r_i^\eta = [\sqrt{(x - x_i)^2 + (y - y_i)^2}]^\eta$

$$\overline{\psi}_i(\boldsymbol{x}) = \sum_{j=1,j\neq i}^{N_b+N_{inside}} \overline{R}_i(\boldsymbol{x})\lambda_j(\boldsymbol{x}_i) = \overline{\boldsymbol{R}}^T(\boldsymbol{x})\boldsymbol{\lambda}(\boldsymbol{x}_i) \tag{11}$$

$$\overline{R}_i(\boldsymbol{x}) = \varphi(\boldsymbol{x})R_i(\boldsymbol{x}) + (1 - \varphi(\boldsymbol{x}))N_i(\boldsymbol{x}) \tag{12}$$

The shape function $\overline{\psi}_i(\boldsymbol{x})$ remains continuous all over the domain. It performs similar to conventional elements on the boundary and acts as meshfree methods inside the element. The ramp function $\varphi(\boldsymbol{x})$ is a C^0 continuous function. Here, the following ramp function is adopted,

$$\varphi(\boldsymbol{x}) = \varphi(x{\cdot}y) = (1 - x^2)(1 - y^2) \tag{13}$$

The unknown vector of coefficients (λ) can then be computed,

$$\lambda(x_m) = \overline{R}^{-1}(x_m)\overline{\psi}_i(x_m) = \overline{R}^{-1}(x_m)\delta_{mi} \tag{14}$$

where x_m is the position of a node.

Moreover, in order to ensure the partition of unity (PU) condition for the derived shape functions, the difference of 1 and the sum of shape functions is distributed over all the shape functions. As a result, the summation of all shape functions becomes equal to one, and the Kronecker delta condition is satisfied:

$$\overline{\overline{\psi}}_i(\boldsymbol{x}) = \overline{\psi}_i(\boldsymbol{x}) + \frac{1}{N_b + N_{inside}}\Delta \tag{15}$$

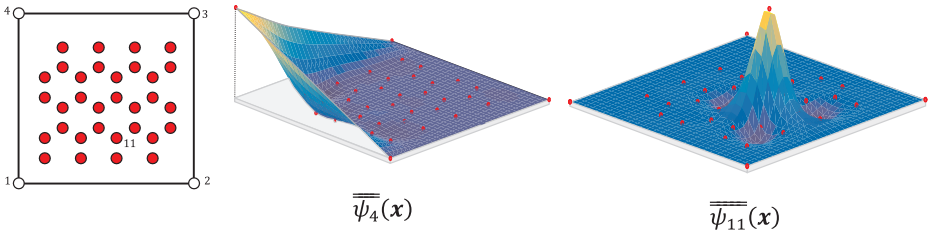

Fig. 6. Shape functions of two nodes of a variable node multiscale element of graphene.

$$\Delta = 1 - \sum_{i=1}^{N_b+N_{inside}} \overline{\psi}_i(x) \tag{16}$$

where $\overline{\overline{\psi}}_i(x)$ is the modified VN shape function which satisfies the PU condition. To better visualize the differences of modified shape functions, Fig. 6 shows the shape functions of a variable node multiscale element of graphene [44].

For details of the formulation of the variable node element and its performance in single scale applications, see [35].

2.4. Examining the validity of the Cauchy-Born rule in VNMM

To examine the validity of the Cauchy-Born rule in VNMM, a simple model of 126 atoms is stretched along the y-axis and analyzed by the molecular statics method (MS) with the embedded atom model (EAM) potential to determine its final correct position, as depicted in Fig. 7. The results of the molecular static simulation are used as a benchmark to examine the results of variable node multiscale element.

The problem is modeled in two extreme cases: a quadrilateral 5-node variable node multiscale element and a 130-node VN multiscale element (see Fig. 8), both based on the TPS radial basis function ($\eta = 0.8$) and the parabolic ramp function. The finite element analysis is performed for both cases and the new positions of atoms (constrained atoms) beneath the 5-node variable node element are determined via the Cauchy-Born rule.

All nodes of the variable node multiscale element coincide with the underneath atoms. In the case of 5-node variable node element, if there is an atom beneath the variable node multiscale element, where no corresponding node exists in the same position, the exact position of the atom can be computed by CBR. The relative error of displacement of the constrained (gray) atoms (shown in Fig. 8a) is calculated by Eq. (17),

$$error = \frac{||x^f_{VNMM} - x^f_{MS}||}{|||x^f_{MS} - x^i_{MS}||} \tag{17}$$

where x is the position vector of atoms, upper indices f and i denote the final and initial positions, respectively and operator $||\bullet||$ represents the norm of vector.

The computed error is 0.077 (7.7%), and more or less similar order of error is obtained for other radial based shape functions and parameters in their well-known recommended range of values [45,46]. Clearly, this amount of error is not acceptable for accurate solutions by the proposed problem.

In the case of 130-node variable node element, the final positions of inside nodes are the same as the solution of molecular statics, and the relative error according to Eq. (17) approaches to zero.

In general, the Cauchy-Born rule in the presence of RBF based shape functions is not accurate enough. The reason can be attributed to the fact that the radial basis shape functions generate nonlinear shape functions, with non-uniform distribution of deformation gradient on the element. The type of the ramp function and its influence domain are expected to affect the validity of the Cauchy-Born rule, which is the subject of an independent study.

Since the underneath atoms cannot generally follow the Cauchy-Born rule, they should be given freedoms in both directions. In this case, all atoms under the variable node multiscale element are considered as the nodes of the variable node element, and they will obey the main formulation of the element to minimize the energy of the whole domain. Therefore, in this problem, the 130-node variable node multiscale element (Fig. 8b), should be used instead of the 5-node variable node multiscale element (Fig. 8a).

3. Numerical simulations

In this section, three different examples are comprehensively

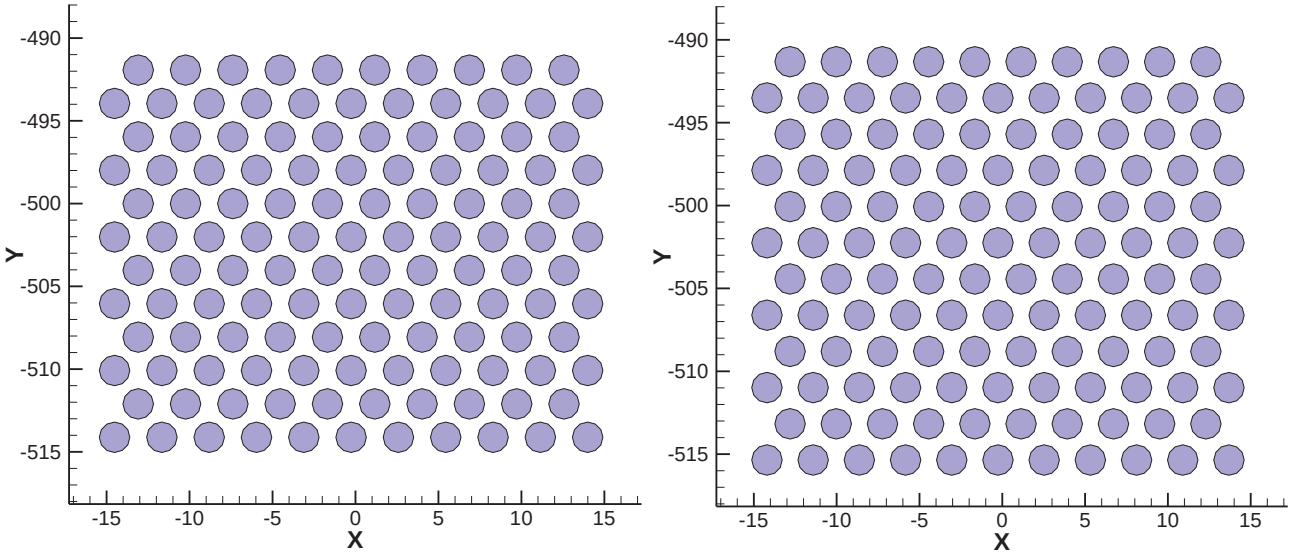

Fig. 7. Molecular static simulation, (right) initial relaxed state, (left) after applied displacement.

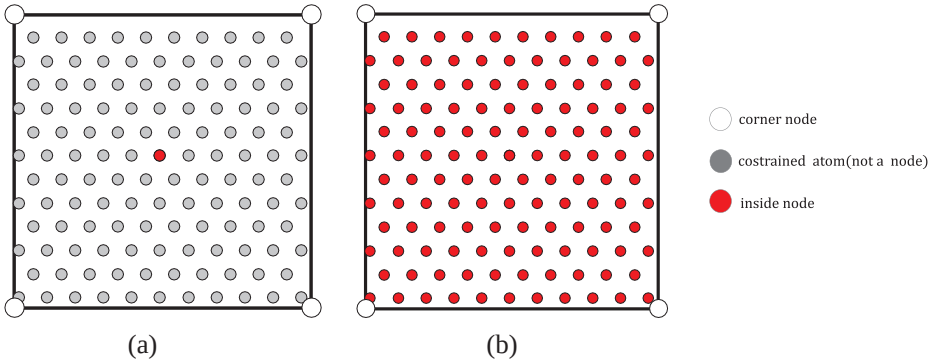

Fig. 8. Variable node multiscale element (a) 5-node, (b) 130-node.

examined to demonstrate the accuracy and efficiency of the proposed approach. In the first two examples, two inhomogeneous compositions of materials are considered. For the sake of simplicity, in the first example, a one-dimensional chain subjected to a uniform loading is simulated. Then, a uniform loading on a two-dimensional plate is simulated in the second example. In the third example, the method is adopted to solve a rather complicated fracture mechanics problem.

3.1. 1D nonhomogeneous bar

A nonhomogeneous chain consisting of 5 copper atoms at the left and 5 Nickel atoms on the right side, as shown in Fig. 9, is considered. The chain is fixed on the left side and is being stretched on the right side with a prescribed displacement. Since the chain is bi-material, a non-uniform distribution of displacement is expected. Despite being a geometrically simple setup, it can well demonstrate the accuracy and power of the proposed approach.

The many-body Rafii-Tabar-Sutton long-range pair potential [47] with the nearest-neighbor interactions rule is utilized to accurately calculate the force-field between atoms in the interface. The mathematical form of the potential is as,

$$\begin{aligned} U^{RTS} = {} & \frac{1}{2}\sum_i \sum_{j\neq i} \hat{p}_i\hat{p}_j V^{AA}(r_{ij}) + (1-\hat{p}_i)(1-\hat{p}_j)V^{BB}(r_{ij}) \\ & + [\hat{p}_i(1-\hat{p}_j) + \hat{p}_j(1-\hat{p}_i)]V^{AB}(r_{ij}) \\ & - d^{AA}\sum_i \hat{p}_i\left[\sum_{j\neq i}\hat{p}_j\phi^{AA}(r_{ij}) + (1-\hat{p}_j)\phi^{AB}(r_{ij})\right]^{\frac{1}{2}} \\ & - d^{BB}\sum_i (1-\hat{p}_i)\left[\sum_{j\neq i}(1-\hat{p}_j)\phi^{BB}(r_{ij}) + \hat{p}_i\phi^{AB}(r_{ij})\right]^{\frac{1}{2}} \end{aligned} \tag{18}$$

where r_{ij} is the distance between two atoms, $\hat{p}_i$ is set to 1 and 0 for copper and nickel atoms, respectively, while $\hat{p}_j$is equal to one and zero for nickel and copper atoms, respectively. Functions $V^{\alpha\beta}$ and $\phi^{\alpha\beta}$ are defined as,

$$V^{\alpha\beta}(r_{ij}) = \epsilon^{\alpha\beta}\left[\frac{a^{\alpha\beta}}{r_{ij}}\right]^{n_{\alpha\beta}} \tag{19}$$

$$\phi^{\alpha\beta}(r_{ij}) = \epsilon^{\alpha\beta}\left[\frac{a^{\alpha\beta}}{r_{ij}}\right]^{m_{\alpha\beta}} \tag{20}$$

Other coefficients are listed in Table 2.

In the case of alloy interaction, in which two different atomic types are engaged, Eqs. (21)–(26) are applied:

Fig. 9. 1D nonhomogeneous chain.

Table 2
Raffi-Tabar-Sutton potential parameters [47]

Atom	m	n	ϵ(eV)	a (Å)	c
Copper	6	9	12.328e-3	3.61	39.432
Nickel	6	9	15.707e-3	3.52	39.432

$$V^{\alpha\beta} = \sqrt{V^{\alpha\alpha}V^{\beta\beta}} \tag{21}$$

$$\phi^{\alpha\beta} = \sqrt{\phi^{\alpha\alpha}\phi^{\beta\beta}} \tag{22}$$

$$m^{\alpha\beta} = \frac{1}{2}(m^{\alpha\alpha} + m^{\beta\beta}) \tag{23}$$

$$n^{\alpha\beta} = \frac{1}{2}(n^{\alpha\alpha} + n^{\beta\beta}) \tag{24}$$

$$a^{\alpha\beta} = \sqrt{a^{\alpha\alpha}a^{\beta\beta}} \tag{25}$$

$$\epsilon^{\alpha\beta} = \sqrt{\epsilon^{\alpha\alpha}\epsilon^{\beta\beta}} \tag{26}$$

First, the chain is relaxed by the Rafii-Tabar-Sutton potential. The relaxed position of 10 atoms, presented in Table 3, is considered as the initial configuration for both the molecular statics and the proposed variable node multiscale methods. The chain undergoes a 3% strain and the results of molecular statics simulation are assumed as the benchmark.

To show the accuracy of VNMM, 3 different setups are examined. All setups are displacement controlled one-dimensional models with a variable node element in the center. Setup 1 has only one VN element, while setups 2 and 3 have 2 conventional bar elements and a one-dimensional variable node multiscale element (see Fig. 10).

All three setups are constrained at the left edge. First, the finite element solutions of the models (u^{coarse}) are computed, and then the fine displacement (u^{fine}) of inside nodes/atoms are calculated from Eq. (8).

The final correct position is the sum of two results, as shown with the solid line in Fig. 11. It is observed that the fine displacement of atoms beneath the conventional bar elements is zero and their total and coarse displacements are equal. This is due to the fact that these atoms obey the CB rule and are located in their final correct position, while the displacement of inside nodes of VN element is not necessarily equal to the total final displacement (see Fig. 12).

After minimizing the energy of inside nodes/atoms, the error in the final position of atoms is calculated from:

$$error\ \ of\ \ final\ \ position = \frac{\boldsymbol{x}^f_{VNMM} - \boldsymbol{x}^f_{MS}}{relaxed\ \ lattice\ \ spacing} \tag{27}$$

where $\boldsymbol{x}^f_{VNMM}$ and $\boldsymbol{x}^f_{MS}$ are the final positions of atoms in VNMM and MS, respectively. The relaxed lattice spacings for Copper and Nickel are 2.0935 Å and 2.0413 Å, respectively.

Fig. 13 depicts the error of final positions of atoms in terms of the

Table 3
Initial and 3% strained positions of atoms according to the molecular statics solution.

Atom	1	2	3	4	5	6	7	8	9	10
Initial position (Å)	0	2.09	4.18	6.28	8.37	10.44	12.48	14.52	16.56	18.60
Final position − 3% applied strain (MS)	0	2.16	4.33	6.50	8.66	10.79	12.88	14.98	17.07	19.16

initial position of atoms (x-axis). Accordingly, the maximum error is about 1% for setup 3, and it reduces as the number of inside nodes/atoms increases (setup2 and setup1). For the setup 1, which all atoms have independent degrees of freedom, the error in final displacement is less than 10^{-6} percent; showing an outstanding agreement with the molecular statics prediction. It should be noted that, the error of displacement of the first and the last atom should be equal to zero as depicted in Fig. 13. This is due to the fact that the position of the first and last atom is determined with the applied Dirichlet boundary condition in both MS and VNMM simulations (fixed boundary condition).

The amount of stress error (E^s) is defined as:

$$E^s = \left| \frac{\boldsymbol{S}^f_{VNMM} - \boldsymbol{S}^f_{MS}}{\boldsymbol{S}^f_{MS}} \right| \times 100 \tag{28}$$

where $\boldsymbol{S}^f_{VNMM}$ and $\boldsymbol{S}^f_{MS}$ are the final stress values of each atom for VNMM and MS simulations, respectively.

The maximum amount of error is less than 6 percent, which can be attributed to the surface effect of the two boundary atoms (see Fig. 14).

3.2. Uniaxial loading on a 2D plate

In order to further investigate the accuracy and efficiency of proposed VNMM in two-dimensional problems, a benchmark example of uniaxial loading, reported by Beex et al. [48], is studied. Since the model includes a stiff region in the middle, the displacement field around the stiff region is not uniform, which is a great test for the new proposed method.

To better compare the results of VNMM with that of the benchmark, a dimensionless full lattice domain is considered. The vertical and horizontal lattice spacings are considered to be 1 unit length (completely similar to the benchmark). The model consists of 10,201 atoms in which 49 atoms belong to the 6×6 unit length stiff region in the middle. The vertical displacement in the bottom edge of the plate (Γ^1_s) and the horizontal displacement of the left edge (Γ^4_s) are forced to be zero. The prescribed displacement on the right edge (Γ^2_s) is imposed by a Dirichlet boundary condition. The top edge (Γ^3_s) is constrained in a way that the vertical displacement of all nodes of the top edge remain equal. Fig. 15 illustrates the geometry and boundary conditions.

As discussed in the previous section, there is no need to refine the mesh to lattice size in order to couple the fully atomistic region with the continuum one. So, the fully atomistic region is surrounded by an arbitrary mesh, as shown in Fig. 16. The underneath atomic lattices are shown in small solid gray circles while the continuum nodes/atom are depicted with red circles. To have an accurate result near the stiff region, all the atoms in the desired zone, are free to move in X/Y directions, while the movement of other atoms follow the deformation gradient of their master triangular element. Those atoms that are allowed to move freely are coincident with internal nodes of the variable node elements.

The initial configuration of the model has a coarse mesh, consisting of 164 triangular elements in the domain. In the setup shown in Fig. 16, the stiff region and its surrounding atoms are modeled with 16 variable node elements (with 9, 12 or 16 inside nodes/atoms). Since each inside node is given two degrees of freedom, no further effort is necessary to adjust the number and arrangement of inside nodes in the variable node element. In this setup, from the existing 10,201 atoms, only 169 atoms in the center of the domain are involved in the energy minimization procedure of Eq. (3).

In Fig. 17, which is a close-up view of the region with variable node elements, each element may have a variable number of inside nodes during the analysis. As the analysis is performed, the position of inside nodes is changed, and the inside nodes/atoms near the edges of a VN multiscale element may move from an element to another, as schematically depicted in Fig. 17. Each node is given two degrees of freedom (in x and y-directions). The white nodes are the corner nodes of conventional triangular finite elements and variable node elements. The corner nodes of variable node elements do not necessarily possess the same position as of the atoms. The red nodes/atoms, which are inside the variable node elements, are the main links between the finite element method and the molecular statics. The gray points under the conventional triangular finite elements do not have any degrees of freedom and will move by the Cauchy-Born rule.

To be similar to the benchmark reference example, each free atom in the entire domain has interactions only with its nearest neighbors. In other words, atoms in the bulk, edge, and corner regions have 8, 5 and 3 neighboring atoms, respectively [48]. To completely calculate the force field, the following interatomic pair potential is employed,

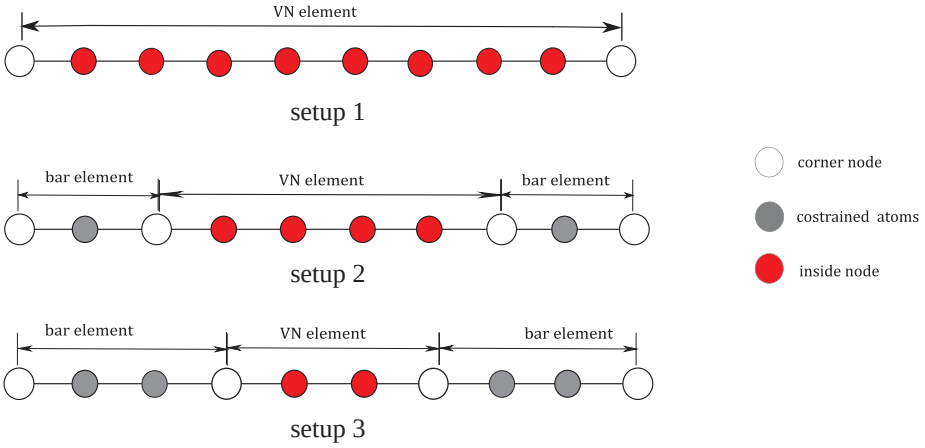

Fig. 10. 1D nonhomogeneous setups.

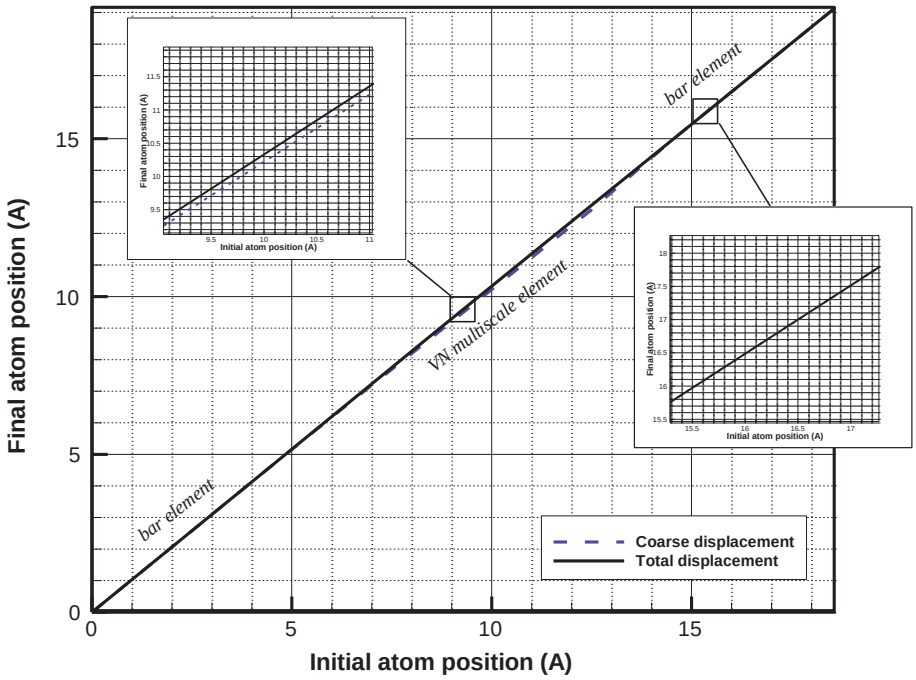

Fig. 11. Displacement decomposition of setup 2.

$$U(r) = \frac{1}{2}\frac{EA}{r_0}(r - r_0)^2 \tag{29}$$

where E is the Young modulus, A is the area and r_0 is the equilibrium initial lattice spacing. Without the loss of generality of the investigation, E, A, and r_0 are set to 1 in this example [48].

On the right edge (Γ_s^2) of the model, shown in Fig. 15, a displacement of 2 unit length is applied and the displacement field over the entire domain is calculated. The displacement is applied in the first iteration and the coarse scale movement of nodes is calculated with the finite element formulation. In the next iterations, the total energy of atoms is minimized. This procedure is terminated when the relative error (E^r) becomes less than an acceptable tolerance,

$$E^r = \frac{|u_2 - u_1|}{|u_1|} \tag{30}$$

where u_2 and u_1 are the displacement vectors of current and previous iterations, respectively.

The accuracy of VNMM is assessed by the molecular static analysis of the full lattice model and its efficiency is compared with the quasi-continuum model. The initial configuration of the quasicontinuum model is illustrated in Fig. 18. The same stiff region is modeled in the center of the plate. Due to oscillatory displacement field around the stiff region, the mesh must be refined to the lattice dimension in that zone. Therefore, the size of the nonlocal zone around the stiff region is assumed larger than the dimensions of the stiff region. To reduce the computational costs, the mesh size is adaptively increased in zones far from the stiff region (see Fig. 18).

To better compare QC with other methods, the fine mesh in the size of the lattice is located just in the nonlocal zone, as shown in Fig. 18b, while, in the MS model, all atoms have degrees of freedom in both

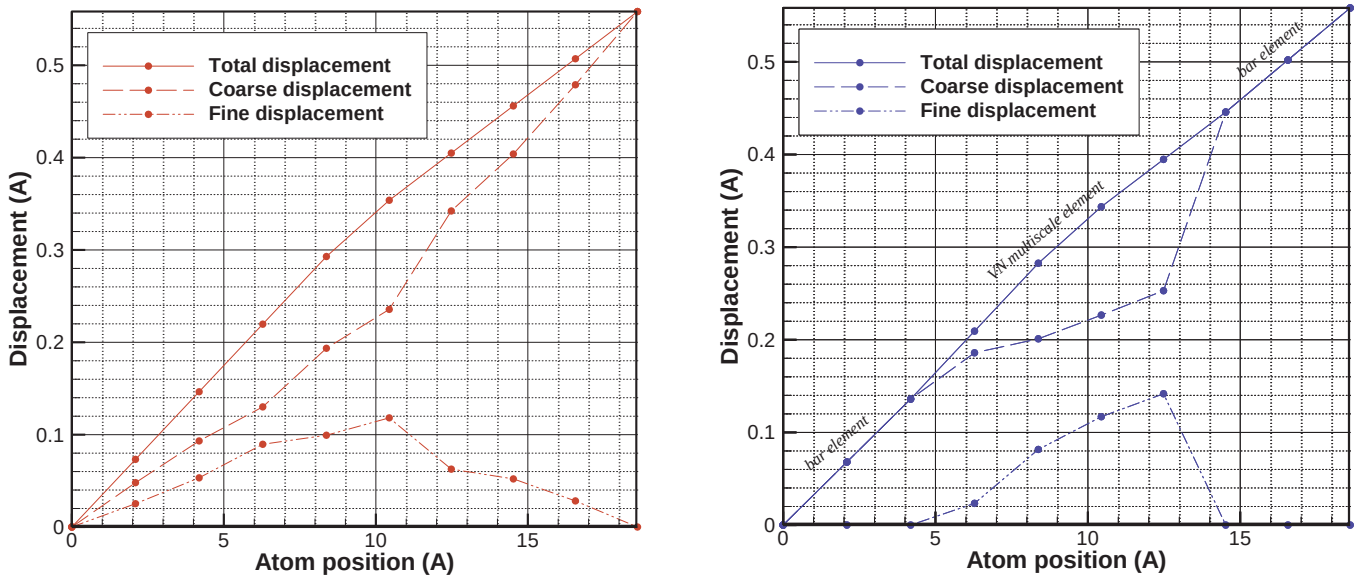

Fig. 12. Displacement decomposition of the one-dimensional bar, (left) Setup 1, (right) Setup 2.

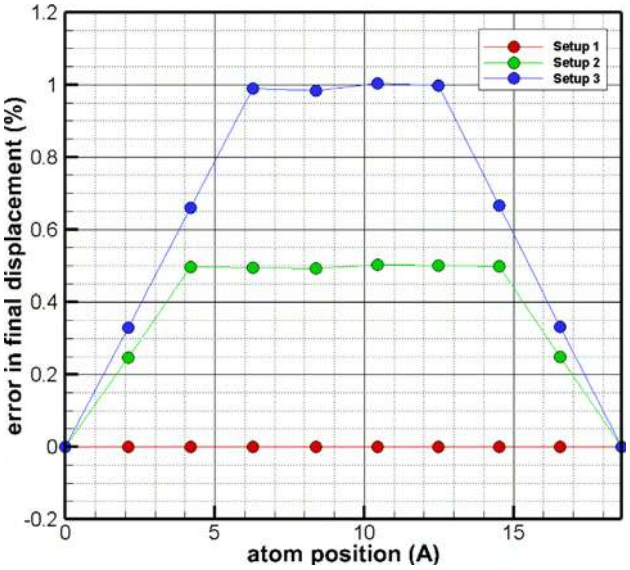

Fig. 13. Error of final position of atoms predicted by VNMM for all three setups.

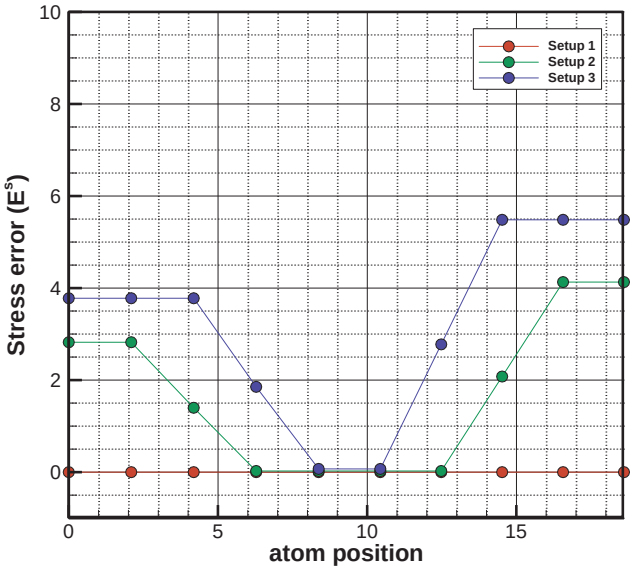

Fig. 14. Error of stress of atoms predicted by VNMM for all three setups.

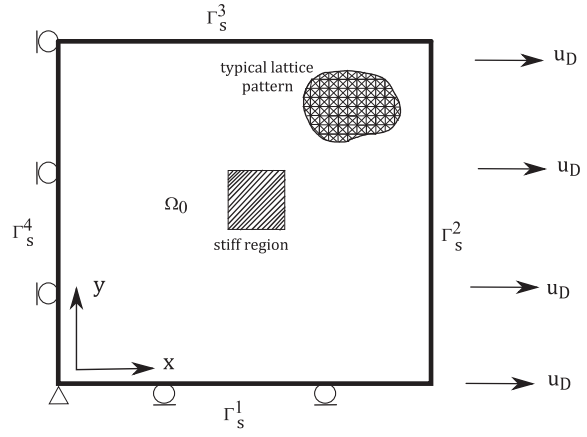

Fig. 15. Geometry and boundary conditions of the 2D uniaxial test.

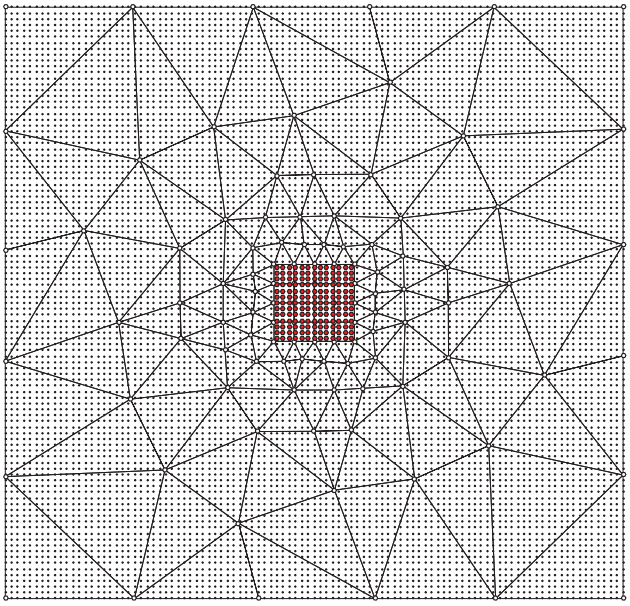

Fig. 16. Adopted VNMM mesh and the fully atomistic region beneath it.

directions and no elements are used.

The QC method uses fixed number of degrees of freedom in each iteration and in each load step, whereas VNMM uses different number of degrees of freedom in iterations associated with coarse and fine displacement calculations. In this problem, VNMM uses 556 degrees of freedom to compute the coarse displacement, and 338 DOFs are used for computing the fine displacement, while QC uses 698 degrees of freedom in each iteration of energy minimization. Computations of coarse and fine displacement in VNMM are not conducted simultaneously in one iteration. As a result, each iteration of QC uses more degrees of freedom than any iterations of coarse or fine displacement calculation of VNMM.

According to Table 4, a large reduction in the number of DOFs is obtained by using a multiscale method such as QC or VNMM. Moreover, VNMM requires fewer degrees of freedom than QC for computing the coarse displacement, while it needs just about half of the DOFs of QC for computing fine displacement. This is due to the fact that unlike VNMM, QC requires mesh refinement inside the nonlocal zone and in its vicinity.

Vertical and horizontal displacements are illustrated in Figs. 19 and 20, respectively. Clearly, the middle inclusion affects the surrounding displacement field, as similarly predicted by VNMM, QC, and the molecular statics.

According to Fig. 21, the maximum difference in displacements of atoms in each direction, predicted by VNMM and molecular statics, is about 0.03 unit length (3% of the lattice spacing), which illustrates the acceptable accuracy of the method.

To better compare the results, variations of the horizontal displacement along the y = 0 line and variations of the vertical displacement along the x = 0 line are depicted in Fig. 22. A very good agreement is observed between the results of VNMM, MS, and QC methods.

3.3. Enriched VNMM for an edge crack problem

In order to simulate a cracked domain consisting of 10,201 atoms, the Heaviside enrichment term, corresponding to the crack edge discontinuity, is used in VNMM. A 100 Å width square plate with a 7 Å long edge crack is considered. The plate is fixed at the bottom edge and a uniform tensile loading is applied on the top edge to simulate a mode I crack problem.

Two different VNMM setups with structured and unstructured

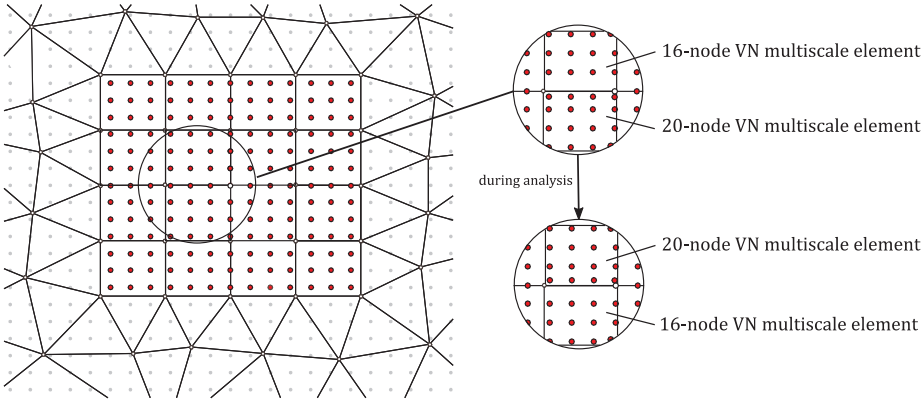

Fig. 17. Modeling of the stiff region by variable node elements.

meshes are proposed as depicted in Fig. 23. The cracked region in both setups is modeled with two variable node multiscale elements (fully includes the crack). The rest of the plate is modeled with conventional triangular finite elements.

The variable node multiscale elements in the vicinity of the crack are enriched with the Heaviside enrichment term. Since the crack tip is located inside one of the variable node multiscale elements, where a full molecular static minimization is performed, no macro based asymptotic enrichment term is used.

To better simulate the crack opening, no interaction between the atoms across the crack sides is considered. In other words, interaction of atoms across the sides of the crack interface is eliminated. The interatomic potential defined by Eq. (25), is used with nominal E and A parameters equal to one. The initial relaxed lattice dimension is 1 Å.

In order to investigate the validity and efficiency of the variable node multiscale method, one fully atomistic setup (solved by molecular statics method) and 3 different multiscale setups (simulated by Quasicontinuum method) are examined. The initial configurations of QC setups are illustrated in Fig. 24.

To better compare VNMM and QC, setup (C) in Fig. 24 with approximately uniform mesh size in zones far from the crack tip, which is similar to VNMM setup with structured mesh (setup A) is considered. The size of the mesh for two other setups increases as the distance of the element from the crack tip increases (similar to setup B). The size of the refined zone near the crack tip in setups (C) and (D) is identical, and is slightly larger in setup (E). Due to the fact that the quasicontinuum method cannot be enriched by the enrichment terms, the crack body is modeled using separated elements with gaps in between. Specifications of the setups are listed in Table 5.

After applying a 2 Å displacement on the top edge, the crack is opened and the displacement field around the crack is perturbed, as shown in Fig. 25 with a tenfold scale for the deformation.

Displacements of atoms in both directions after applying the displacement on the top edge are depicted in Fig. 26.

The relative error of vertical displacement predicted by VNMM with respect to MS is demonstrated in Fig. 27. Clearly, a good agreement is observed, with a maximum error of near 5% (0.05 Å) for setup A of VNMM.

As the plate is further stretched, the vertical stress S_{yy} near the crack tip increases. To show the stress components in atomic scale, the virial stress components are calculated [49],

$$S^{virial}(\mathbf{r}) = \frac{1}{2\Omega}\sum_{j\neq i} \mathbf{r}_{ij} \otimes \mathbf{f}_{ij} \tag{31}$$

where for the proposed potential, the stress components can then be calculated by (32),

$$S^{i}_{\alpha\beta}(r_{ij}) = \frac{1}{2\Omega}\sum_{j\neq i}\left(\frac{1}{r^{ij}}\frac{\partial U}{\partial r^{ij}}(r^{j}_{\alpha} - r^{i}_{\alpha})(r^{j}_{\beta} - r^{i}_{\beta})\right) \tag{32}$$

where lower indices α and β, ranging from 1 to 3, represent three independent directions and the upper index is the atom number.

In order to better demonstrate the accuracy of VNMM in predicting the high gradient nature of stress near the crack tip, Fig. 28 compares variations of S_{22} along the crack for all VNMM, QC and MS setups. Clearly, a very good agreement, both qualitatively and quantitatively, is observed for this complex high gradient response near the crack tip for

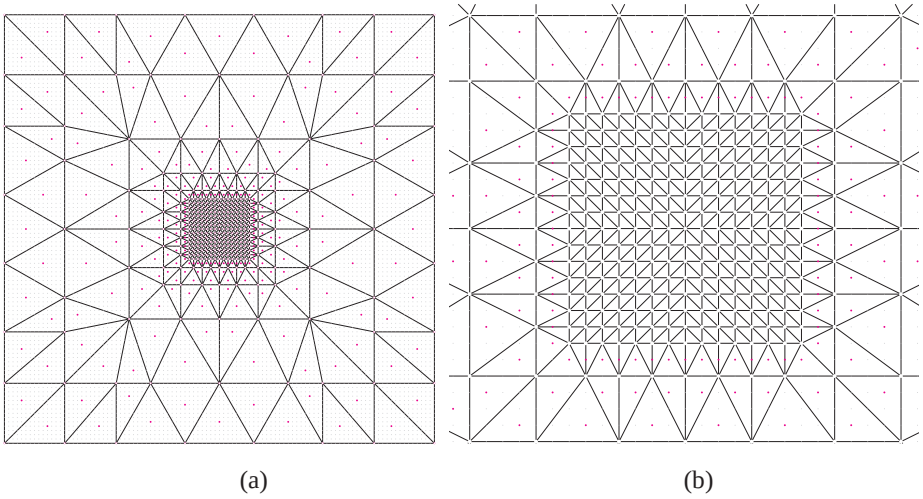

Fig. 18. (a) Initial configuration of the quasicontinuum model, (b) the fine mesh of QC around the stiff region.

Table 4
Specification of adopted MS, QC and VNMM models.

Method	Number of elements	Number of nodes or atoms	Number of DOFs
Molecular Statics	–	10,201	20,402
Quasicontinuum	668	349	698
VNMM	180	278 (for computing u^{coarse}) and 169 (for computing u^{fine})	556 (for computing u^{coarse}) and 338 (for computing u^{fine})

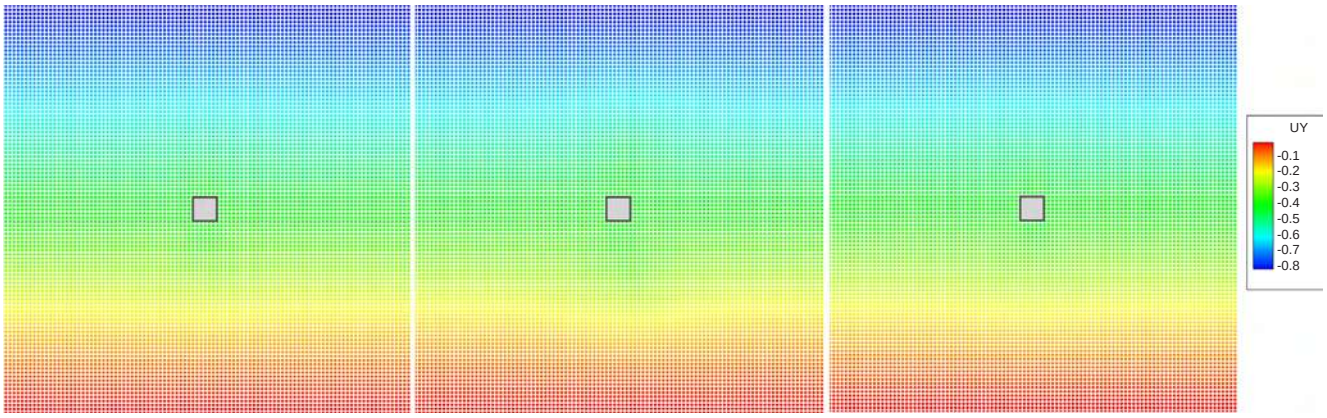

Fig. 19. Vertical displacement contour, (left) MS, (center) VNMM, (right) QC.

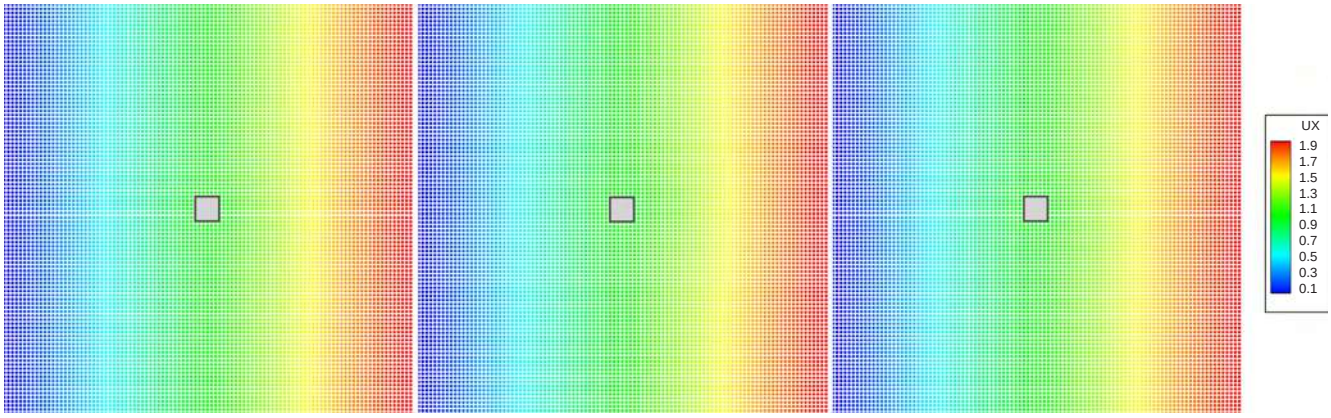

Fig. 20. Horizontal displacement contour, (left) MS, (center) VNMM, (right) QC.

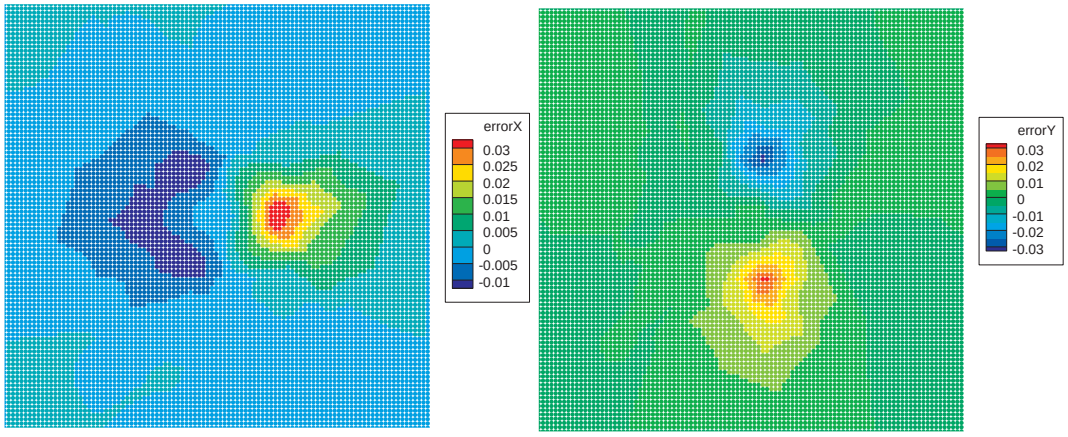

Fig. 21. Difference in displacement fields predicted by VNMM and MS, (left) horizontal displacement, (right) vertical displacement.

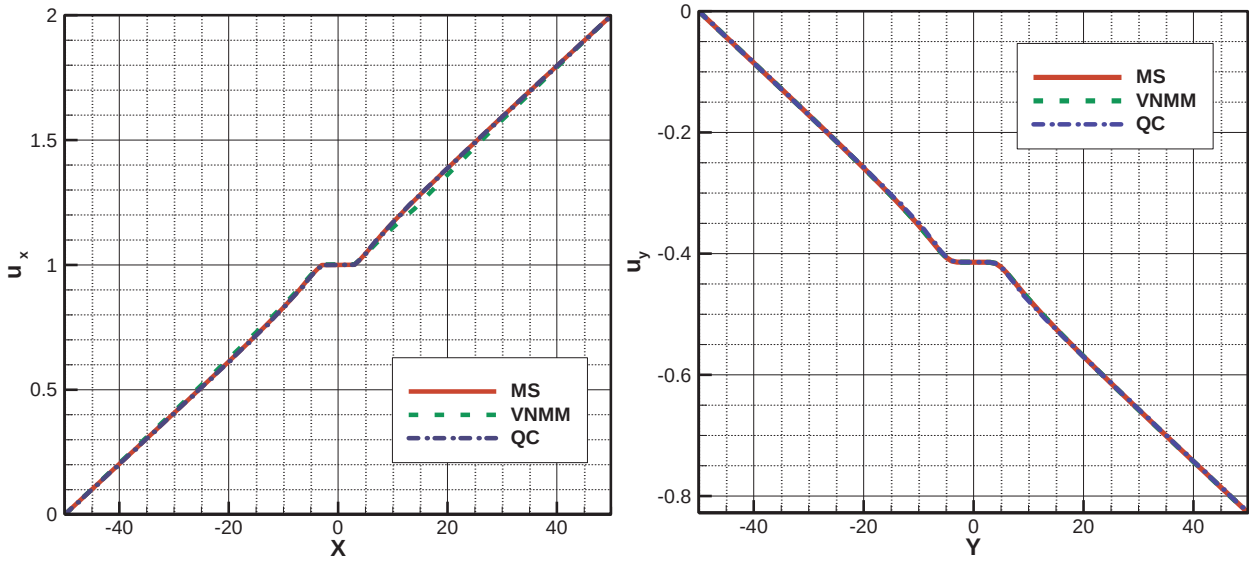

Fig. 22. (left) Horizontal displacement along y = 0, (right) vertical displacement along x = 0.

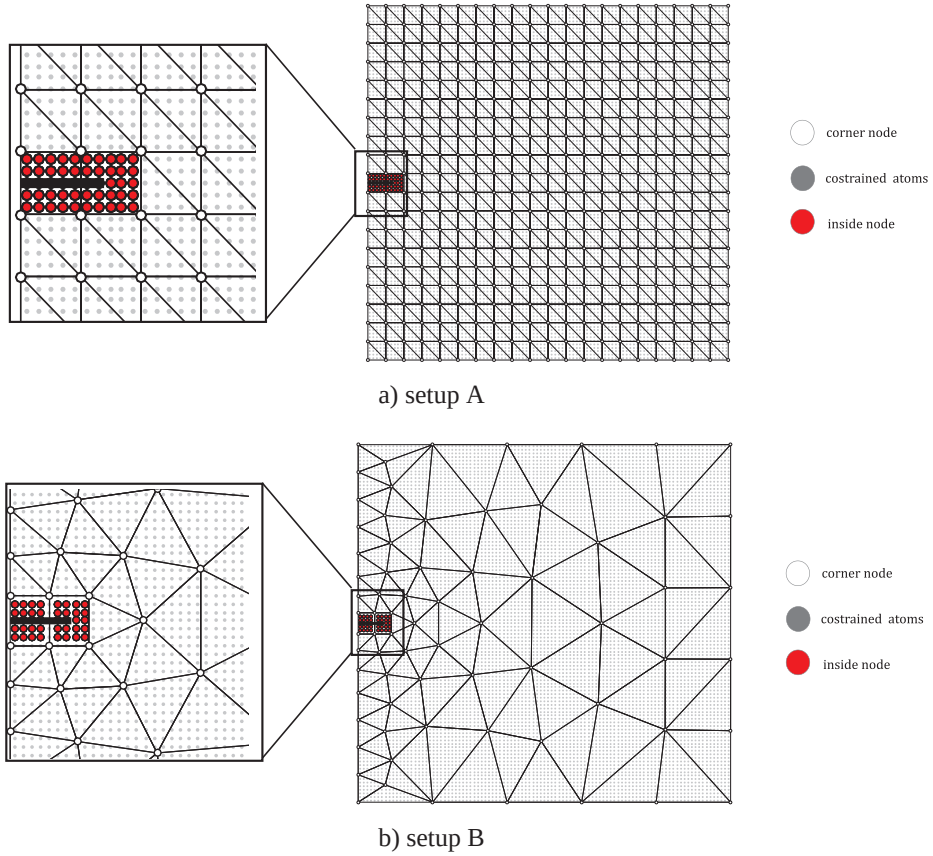

Fig. 23. Initial configurations of two VNMM setups, (a) setup A with structured mesh, (b) setup B with unstructured mesh.

VNMM simulations.

To better show the distribution of error along the crack, a relative error (E_r) based on the vertical stress component is defined:

$$E_r = \frac{|S_{yy}^{VNMM} - S_{yy}^{MS}|}{|S_{yy}^{MS}|} \tag{33}$$

which shows that the maximum error of VNMM is less than 2% near the crack tip and vanishes in the regions far from the crack tip (see Fig. 29).

The overall information of Table 6 shows that increasing the number of degrees of freedom of the QC setup does not lead to further reduction of the errors of vertical stress and displacement below a certain level, while the error of VNMM reduces significantly as the number of degrees of freedom increases. Moreover, comparison of QC and VNMM with nearly equal number of degrees of freedom (setups A and D) shows that the error of VNMM is about one-sixteenth and half of the error of QC setups for vertical stress and vertical displacement, respectively.

Moreover, the runtime of VNMM method is significantly lower than

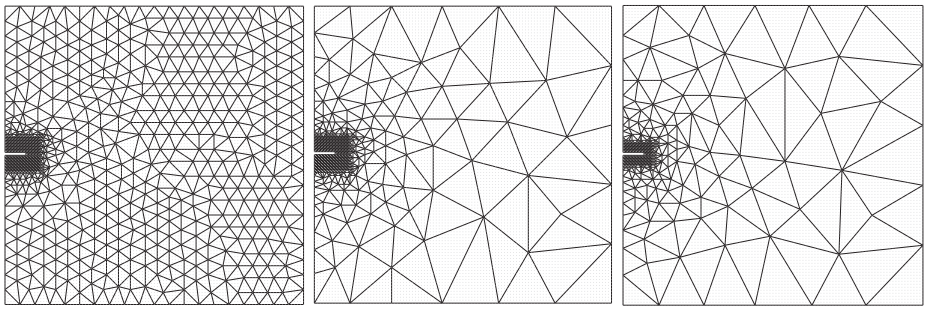

a) setup C (QC) b) setup D (QC) c) setup E (QC)

Fig. 24. Initial configurations of an edge crack plate simulated by QC models.

Table 5
Setups specifications.

Multiscale method	Setup	Number of atoms	Number of nodes	Number of DOFs	Number of elements	Approximate size of elements far from the crack (A)
MS	–	10,201	–	20,402	–	–
VNMM	A	10,201	465	942	380	5
VNMM	B	10,201	111	234	108	20
QC	C	10,201	818	1636	1265	5
QC	D	10,201	450	900	576	20
QC	E	10,201	300	600	404	20

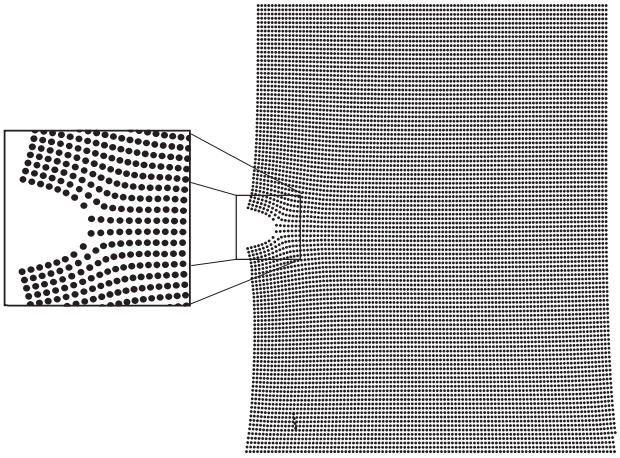

Fig. 25. Deformed configuration of the edge crack (a tenfold scale for deformation).

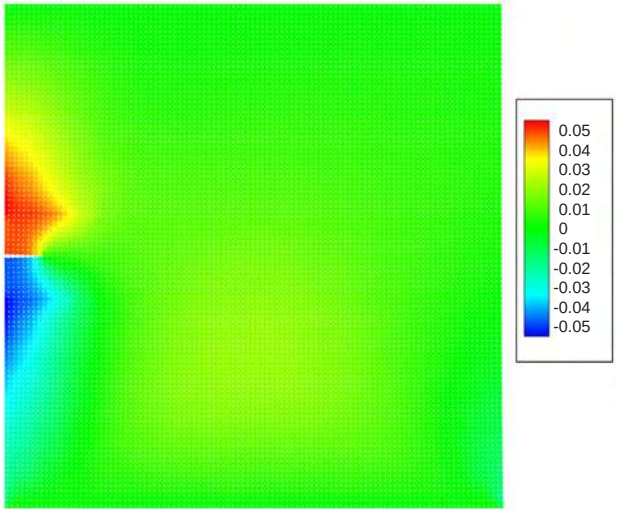

Fig. 27. Error of final position with respect to the lattice parameter, predicted by VNMM.

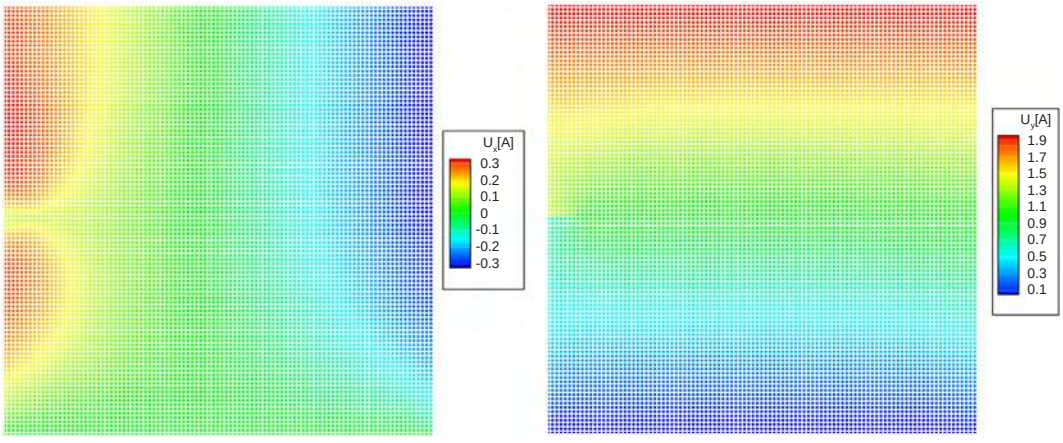

Fig. 26. (left) Horizontal displacement, (right) vertical displacement.

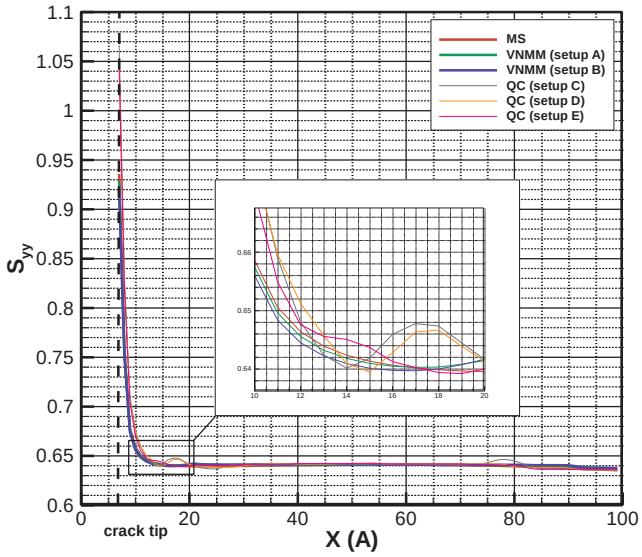

Fig. 28. S_{yy} distribution along the crack.

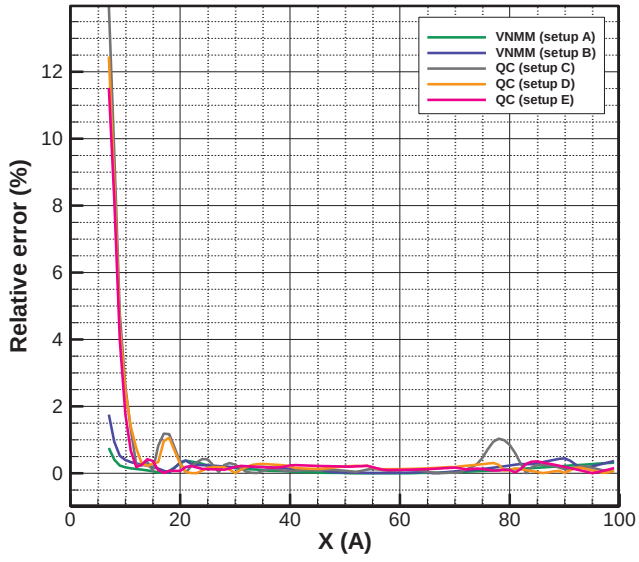

Fig. 29. S_{yy} relative error along the crack.

Table 6
Summery of error for different multiscale methods.

Multiscale method	Setup	Number of DOFs	Maximum error of vertical stress (%)	Maximum error of vertical displacement (%)
VNMM	A	942	0.75	3.26
VNMM	B	234	1.75	5.14
QC	C	1636	13.97	4.79
QC	D	900	12.46	6.8
QC	E	600	11.52	6.66

MS, due to huge reduction of degrees of freedom. The analysis runtime, on a 2.8 GHz-Core i7 CPU with 8.00 GB RAM is 6.52, 6.78 and 28.9 s for setup (A) of VNMM, setup (D) of QC and MS simulations, respectively.

3.4. Lomer dislocation dipole

To completely show the accuracy of VNMM in using long range potentials, a 400 Å width square plate of aluminum atoms with a dipole of Lomer dislocations [50] is simulated. The crystallographic direction

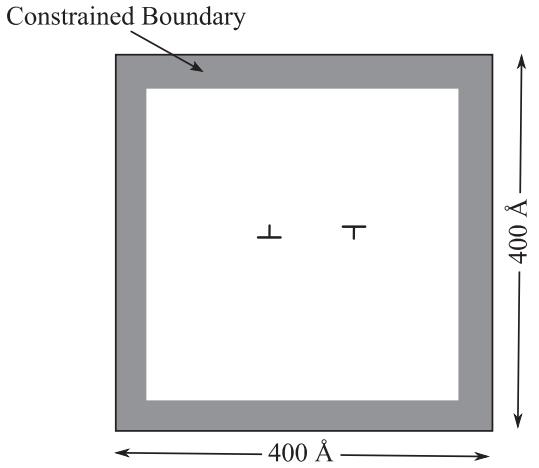

Fig. 30. Schematic illustration of the Lomer dipole setup.

[1 1 0] and [0 0 1] of aluminum atoms are along the global X and Y directions, respectively. All sides of the setup are constrained and a specific amount of displacement proportional to y-coordinate of the boundary is applied along the X direction. Two dislocations (dipoles) are placed in the center of the plate and they are 40 Å away from each other (see Fig. 30)

A VNMM setup, which consists of 182 conventional 3-nodded elements and 25 variable node multiscale elements, is created. The VNMM setup has 1217 nodes with 2434 degrees of freedom. The model contains 27,867 atoms. The atoms under the conventional finite elements, depicted with gray dots in Fig. 31, obey the CB rule and the others, shown with red dots, do have independent degrees of freedom. To better investigate the accuracy of VNMM model, the results are compared with the results of molecular statics setup.

A shear strain is applied on the boundary of the model based on Eq. (34)

$$u_y = \gamma Y \tag{34}$$

where Y represents the coordinate of boundary nodes along the y-axis and γ is the magnitude of applied shear. The interatomic force between the atoms is governed by the embedded atom model (EAM) [51].

After applying 4% of strain, the horizontal and vertical displacements of the atoms are calculated, as presented in Figs. 32 and 33 for MS and VNMM setups, respectively.

The results of VNMM shows a good agreement with those of MS, with a maximum difference of less than 1%. The contour of vertical displacement error is depicted in Fig. 34.

To better demonstrate the accuracy of the VNMM method, the analytical solution for the vertical displacement of the two dislocations problem [52] is adopted:

$$U_y = -\frac{b}{2\pi}\left[\frac{1-2\nu}{4(1-\nu)}\ln((x-x_d)^2+(y-y_d)^2) + \frac{(x-x_d)^2-(y-y_d)^2}{4(1-\nu)((x-x_d)^2+(y-y_d)^2)}\right] \tag{35}$$

where x_d and y_d are the coordinates of the dislocation core in global X and Y directions, respectively, b is the Burgers' vector and ν is the Poisson's ratio. Fig. 35 shows the results of the analytical solution computed by Eq. (35).

The amount of error of the VNMM results with respect to the analytical solution for the vertical displacement is computed from Eq. (36)

$$E_{VNMM} = \frac{|U_y^{VNMM} - U_y^{analytical}|}{lattice\ \ constant} \times 100 \tag{36}$$

where U_y^{VNMM} and $U_y^{analytical}$ are the results of VNMM and analytical

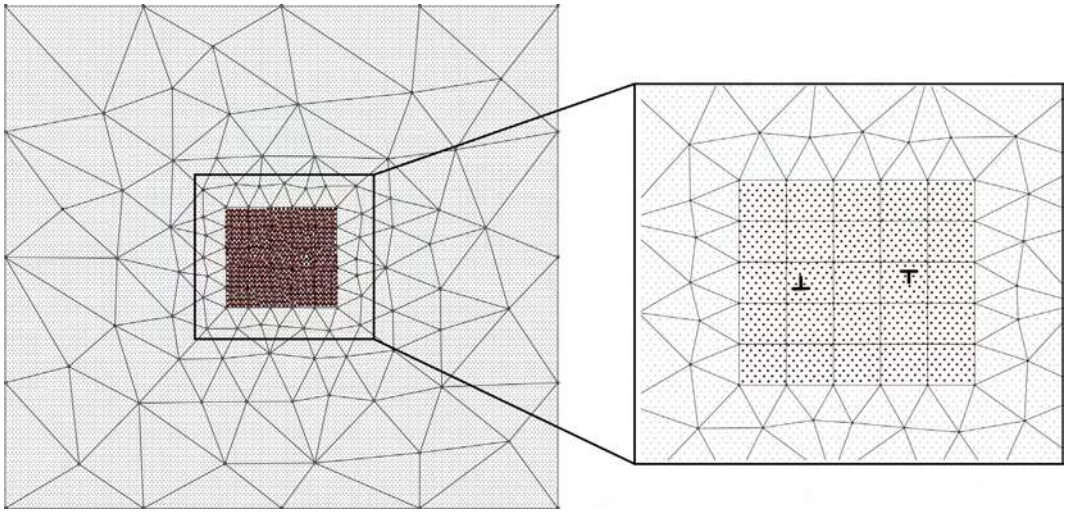

Fig. 31. Lomer dipoles setups, (left) VNMM setup, (right) VNMEs close view.

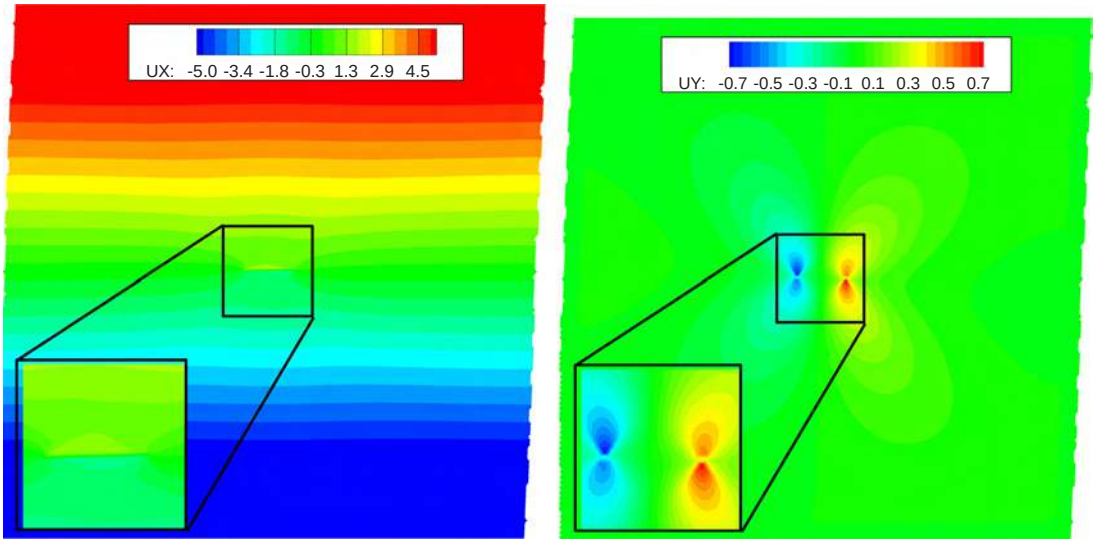

Fig. 32. Results of molecular statics simulations, (left) horizontal displacement, (right) vertical displacement.

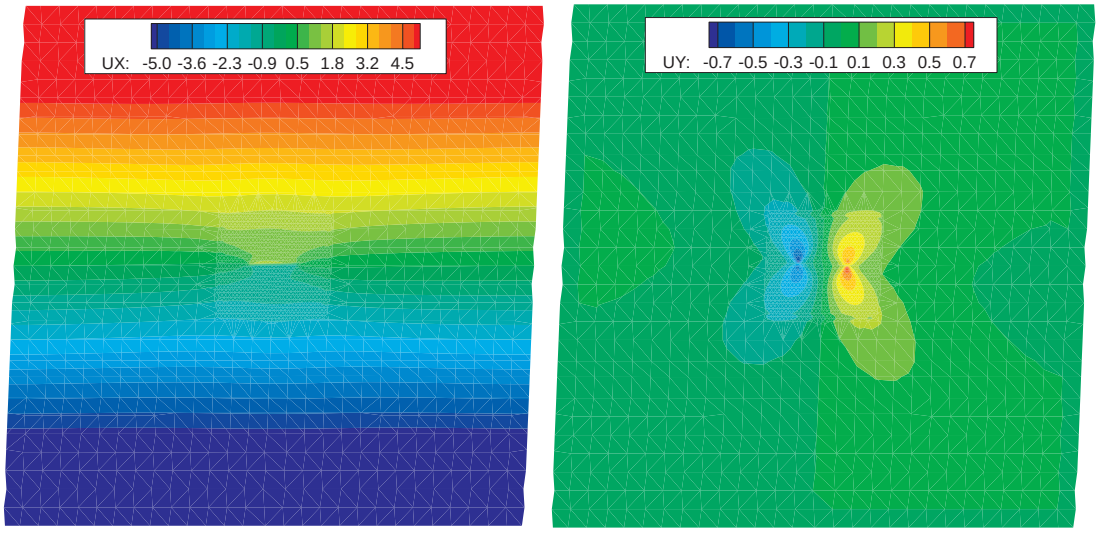

Fig. 33. Results of VNMM simulations, (left) horizontal displacement, (right) vertical displacement.

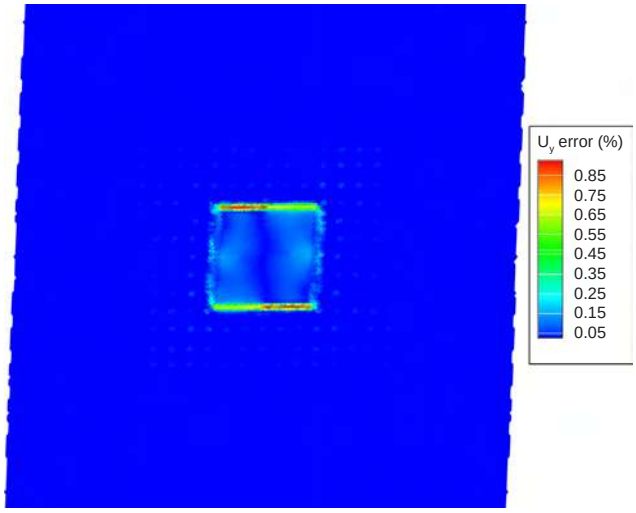

Fig. 34. Error of the vertical displacement of VNMM.

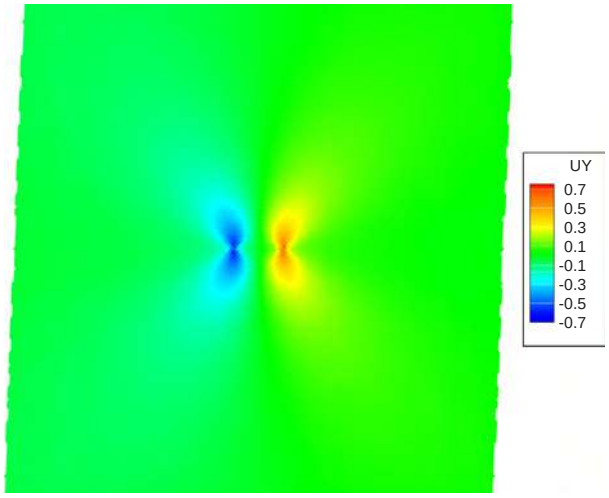

Fig. 35. Results of the vertical displacement obtained from analytical solutions.

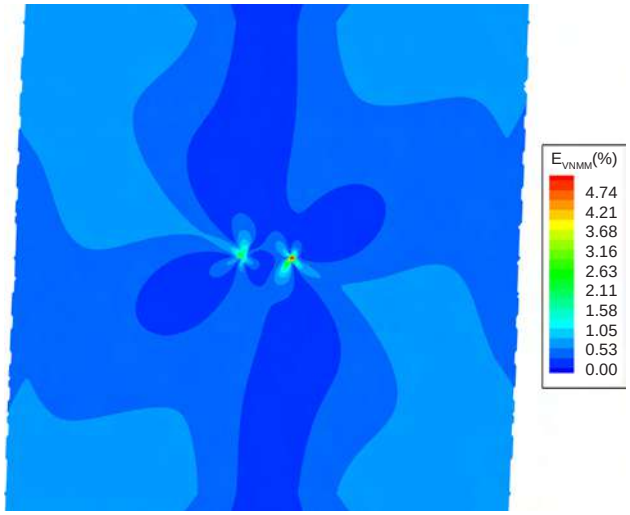

Fig. 36. Error of the vertical displacement.

solution, respectively, and the lattice constant for aluminum is 4.032 Å. Contours of E_{VNMM}, as depicted in Fig. 36, shows a maximum error of less than 5%, which confirms a good agreement and the level of accuracy of VNMM in this simulation.

4. Conclusion

Reduction of computational costs while preserving the desired accuracy in a multiscale problem is of outmost important. In the new proposed approach, the variable node multiscale method (VNMM) combines the flexibility and accuracy of meshfree methods with the simplicity of finite element method to create an element which could be placed in a zone, where the high accuracy of atomic-based methods is required.

VNMM enables the model to estimate the coarse displacement of atoms with just a limited number of degrees of freedom in the platform of FEM, and the fine displacements are calculated based on the use of interatomic potential in the required zones with few numbers of inside nodes/atoms. Decomposition of total displacement into two independent coarse and fine displacements, enables VNMM to reduce the number of DOFs, as the simulation is performed. This is due to the fact that the total number of degrees of freedom for computing the fine displacement is significantly less than that of the coarse displacement calculations.

Adjustable positions of the inside nodes of the variable node multiscale element provide a platform to arrange any materials structure and to eliminate the need for mesh refinement.

The method can potentially be applied on any extension of FEM. As a result, all forms of solid material constitutive models in the continuum zone with known interatomic potential can be similarly implemented and easily be engaged with the molecular zone. It is important to model only materials which obey the Cauchy-Born rule. As a result, the present VNMM modeling is not suitable for amorphous materials. Nevertheless, utilization of standard CB rule for crystalline materials, higher order Cauchy-Born rule for complex lattices and nanotubes does not alter the concept and platform of VNMM algorithm. Moreover, while the Cauchy-Born rule is no longer valid in VNMM, it can be used in the neighboring elements to reduce the computational costs by sharply reducing the number of degrees of freedom.

Data availability

The datasets generated during the current study are available from the corresponding author on reasonable request.

CRediT authorship contribution statement

Omid Alizadeh: Conceptualization, Methodology, Software, Validation, Visualization, Writing - original draft. **Soheil Mohammadi:** Conceptualization, Methodology, Supervision, Writing - review & editing.

Acknowledgments

The authors gratefully acknowledge the High-Performance Computing Laboratory (HPC Lab), University of Tehran for the technical support. The authors express their thanks to Mr. O. Rokos and L. Beex for their open source quasicontinuum code.

References

[1] M. Jebahi, F. Dau, J.-L. Charles, I. Iordanoff, Multiscale modeling of complex dynamic problems: an overview and recent developments, Arch. Comput. Methods Eng. 23 (1) (2016) 101–138.
[2] J. Fish, Bridging the scales in nano engineering and science, J. Nanopart. Res. (2006) 577–594.
[3] H. Talebi, M. Silani, S.P.A. Bordas, P. Kerfriden, T. Rabczuk, A computational

library for multiscale modeling of material failure, Comput. Mech. 53 (2014) 1047–1071.
[4] E.B. Tadmor, R.E. Miller, Modeling Materials; Continuum, Atomistic and Multiscale Techniques, Cambridge University Press, New York, 2011.
[5] E.B. Tadmor, M. Ortiz, R. Phillips, Quasicontinuum analysis of defects in solids, Philos. Mag. A (1996) 1529–1563.
[6] R.Z. Qiu, Y.C. Lin, T.H. Fang, L.-R. Tsai, The crack growth and expansion characteristics of Fe and Ni using quasi-continuum method, Mater. Res. Express 4 (3) (2017).
[7] T. Xu, J. Fan, R. Stewart, X. Zeng, A. Yao, Quasicontinuum simulation of brittle cracking in single-crystal material, Cryst. Res. Technol. 52 (3) (2017).
[8] I. RingdalenVatne, E. stby, C. Thaulow, D. Farkas, Quasicontinuum simulation of crack propagation in bcc-Fe, Mater. Sci. Eng., A 528 (15) (2011) 5122–5134.
[9] T. Zhou, X. Yang, C. Chen, Quasicontinuum simulation of single crystal nano-plate with a mixed-mode crack, Int. J. Solids Struct. 46 (9) (2009) 1975–1980.
[10] S. Huang, C. Zhou, Modeling and simulation of nanoindentation, JOM (2017).
[11] O. Alizadeh, G. Toloee Eshlaghi, S. Mohammadi, Nanoindentation simulation of coated aluminum thin film using quasicontinuum method, Comput. Mater. Sci. (2016).
[12] K. Mikes, M. Jirasek, Quasicontinuum method extended to irregular lattices, Comput. Struct. (2017).
[13] P. Chen, Y. Shen, Nanocontact between BCC tungsten and FCC nickel using the quasicontinuum method, Int. J. Solids Struct. 45 (24) (2008) 6001–6017.
[14] J.S. Amelang, D.M. Kochmann, Surface effects in nanoscale structures investigated by a fully-nonlocal energy-based quasicontinuum method, Mech. Mater. 90 (2015) 166–184.
[15] L.M. Dupuy, E.B. Tadmor, R.E. Miller, R. Phillips, Finite-temperature quasicontinuum: molecular dynamics without all the atoms, Phys. Rev. Lett. 95 (2005).
[16] E. Tadmor, F. Legoll, W. Kim, L. Dupuy, R. Miller, Finite-temperature quasi-continuum, Appl. Mech. Rev. 65 (1) (2013).
[17] X. Wang, X. Guo, Numerical simulation for finite deformation of single-walled carbon nanotubes at finite temperature using temperature-related higher order Cauchy-Born rule based quasi-continuum model, Comput. Mater. Sci. (2012) 273–283.
[18] L. Beex, O. Rokoš, J. Zeman, S. Bordas, Higher-order quasicontinuum methods for elastic and dissipative lattice models: uniaxial deformation and pure bending, GAMM-Mitteilungen 38 (2) (2015) 344–368.
[19] J.S. Amelang, G.N. Venturini, D.M. Kochmann, Summation rules for a fully-nonlocal energy-based quasicontinuum method, J. Mech. Phys. Solids (2015) 378–413.
[20] L. Beex, R. Peerlings, M. Geers, Central summation in the quasicontinuum method, J. Mech. Phys. Solids 70 (2014) 242–261.
[21] C. Ortner, L. Zhang, Atomistic/continuum blending with ghost force correction, SIAM J. Sci. Comput. (2016) A346–A375.
[22] M. Dobson, M. Luskin, An analysis of the effect of ghost force oscillation on quasicontinuum error, Math. Modell. Numer. Anal. 43 (2009) 591–604.
[23] M. Dobson, R. Elliott, M. Luskin, E. Tadmor, A multilattice quasicontinuum for phase transforming materials: cascading Cauchy Born kinematics, J. Comput. Aided Mater. Des. 14 (2007) 219–237.
[24] V. Sorkin, R. Elliott, E.B. Tadmor, A local quasicontinuum method for 3D multilattice crystalline materials: application to shape-memory alloys, Modell. Simul. Mater. Sci. Eng. 22 (2014).
[25] S. Xiao, T. Belytschko, A bridging domain method for coupling continua with molecular dynamics, Comput. Methods Appl. Mech. Eng. 193 (17–20) (2004) 1645–1669.
[26] G.J. Wagner, W.K. Liu, Coupling of atomistic and continuum simulations using a bridging scale decomposition, J. Comput. Phys. 190 (1) (2003) 249–274.
[27] J. Fish, Multiscale Methods: Bridging the Scales in Science and Engineering, Oxford Scholarship Online, 2009.
[28] H. Talebi, M. Silani, T. Rabczuk, Concurrent multiscale modeling of three dimensional crack and dislocation propagation, Adv. Eng. Softw. 80 (2015) 82–92.
[29] W.K. Liu, H.S. Park, D. Qian, E.G. Karpov, H. Kadowaki, G.J. Wagner, Bridging scale methods for nanomechanics and materials, Comput. Methods Appl. Mech. Eng. (2006).
[30] V. Iacobellis, K. Behdinan, Comparison of concurrent multiscale methods in the application of fracture in nickel, J. Appl. Mech. 80 (5) (2013).
[31] D.M. Kochmann, G.N. Venturini, A meshless quasicontinuum method based on local maximum-entropy interpolation, Modell. Simul. Mater. Sci. Eng. (2014).
[32] Q.X. Wang, T.Y. Ng, H. Li, K.Y. Lam, Multiscale simulation of coupled length-scales via meshless method and molecular dynamics, Mech. Adv. Mater. Struct. 16 (1) (2009) 1–11.
[33] P.R. Budarapu, R. Gracie, S.-W. Yang, X. Zhuang, T. Rabczuk, Efficient coarse graining in multiscale modeling of fracture, Theor. Appl. Fract. Mech. 69 (2014) 126–143.
[34] P.R. Budarapu, R. Gracie, S.P. Bordas, T. Rabczuk, An adaptive multiscale method for quasi-static crack growth, Comput. Mech. 53 (6) (2014) 1129–1148.
[35] O. Alizadeh, M. Khodadad, S. Akhavan and S. Mohammadi, A new meshless-based variable-node finite element, (submitted for publication).
[36] J. Ericksen, The Cauchy and Born hypotheses for crystals, Phase Transformations and Material Instabilities in Solids, Academic Press, New York, 1984, pp. 61–77.
[37] E. Marenić, A. Ibrahimbegovic, Multiscale atomistic-to-continuum reduced models for micromechanical systems, Computational Methods for Solids and Fluids, Springer, 2016, pp. 215–244.
[38] P. Steinmann, A. Elizondo, R. Sunyk, Studies of validity of the Cauchy–Born rule by direct comparison of continuum and atomistic modelling, Modell. Simul. Mater. Sci. Eng. 15 (1) (2006).
[39] P. Atkins, J.d. Paula, Atkins' Physical Chemistry, Oxford University Press, 2010.
[40] G. Liu, Mesh Free Methods: Moving Beyond the Finite Element Method, CRC Press, 2002.
[41] R. Hardy, Theory and applications of the multiquadric-biharmonic method 20 years of discovery 1968–1988, Comput. Math. Appl. 19 (8–9) (1990) 163–208.
[42] M.J. Powell, The theory of radial basis function approximation, Adv. Numer. Anal. 2 (1992) 105–210.
[43] M. Powell, The uniform convergence of thin plate splines in two dimensions, Numerische Mathematik 68 (1) (1994) 107–128.
[44] H. Zhu, Graphene; Characterizations, Properties and Applications, Elsevier Inc, 2018.
[45] J. Wang, G. Liu, On the optimal shape parameters of radial basis functions used for 2-D meshless methods, Comput. Methods Appl. Mech. Eng. 191 (2002) 2611–2630.
[46] G. Liu, G. Zhang, Y. Gu, Y. Wang, A meshfree radial point interpolation method (RPIM) for three-dimensional solids, Comput. Mech. 36 (2005) 421–430.
[47] H. Rafii-Tabar, A.P. Sutton, Long range Finnis-Sinclair potentials for f.c.c metalic alloys, Philos. Mag. Lett. (1991) 217–224.
[48] O. Rokoš, L. Beex, J. Zeman, R. Peerlings, A variational formulation of dissipative quasicontinuum methods, Int. J. Solids Struct. 102–103 (2016) 214–229.
[49] S. Shen, S. Atluri, Atomic-level stress calculation and continuum-molecular system equivalence, Comput. Model. Eng. Sci. (2004).
[50] R.E. Miller, E.B. Tadmor, A unified framework and performance benchmark of fourteen multiscale atomistic/continuum coupling methods, Modell. Simul. Mater. Sci. Eng. 17 (5) (2009).
[51] M.S. Daw, M.I. Baskes, Embedded-atom method: derivation and application to impurities, surfaces, and other defects in metals, Phys. Rev. B 29 (12) (1984).
[52] J.P. Hirth, J. Lothe, Theory of Dislocations, Krieger Publishing Company, 1992.